**Title**

Structure-function analysis of *Arabidopsis* TOPLESS reveals fundamental conservation of repression mechanisms across eukaryotes

**Authors**

Alexander R. Leydon[1], Wei Wang[2,†], Hardik P. Gala[1], Sabrina Gilmour[1], Samuel Juarez-Solis[1], Mollye L. Zahler[1], Joseph E. Zemke[1], Ning Zheng[2,3], Jennifer L. Nemhauser[1]

[1]Department of Biology, University of Washington

[2]Department of Pharmacology & [3]Howard Hughes Medical Institute, University of Washington

[†]Present address: Key Laboratory of Plant Stress Biology, State Key Laboratory of Cotton Biology, School of Life Science, Jinming Campus, Henan University, Kaifeng, Henan Province, 475004, PR of China.

**Summary**

The plant corepressor TOPLESS (TPL) is recruited to a large number of loci that are selectively induced in response to developmental or environmental cues, yet the mechanisms by which it inhibits expression in the absence of these stimuli is poorly understood. Previously, we had used the N-terminus of *Arabidopsis thaliana* TPL to enable repression of a synthetic auxin response circuit in *Saccharomyces cerevisiae* (yeast). Here, we leveraged the yeast system to interrogate the relationship between TPL structure and function, specifically scanning for repression domains. We identified a potent repression domain in Helix 8 located within the CRA domain, which directly interacted with the Mediator middle domain subunits Med21 and Med10. Interactions between TPL and Mediator were required to fully repress transcription in both yeast and plants. In contrast, we found that multimer formation, a conserved feature of many corepressors, had minimal influence on the repression strength of TPL.

**Keywords**

Corepressors, Transcriptional Repression, Mediator, Tup1, TOPLESS

41 **Introduction**

42 Control over gene expression is essential for life. This is especially evident during development
43 when the switching of genes between active and repressed states drives fate determination.
44 Mutations that interfere with repression lead to or exacerbate numerous cancers (Wong et al.,
45 2014) and cause developmental defects in diverse organisms (Grbavec et al., 1998; Long et al.,
46 2006), yet many questions remain about how cells induce, maintain, and relieve transcriptional
47 repression. Transcriptional repression is controlled in part by a class of proteins known as
48 corepressors that interact with DNA-binding transcription factors and actively recruit repressive
49 machinery. Transcriptional corepressors are found in all eukaryotes and include the animal
50 SMRT (silencing mediator of retinoic acid and thyroid hormone receptor) and NCoR (nuclear
51 receptor corepressor) complexes (Mottis et al., 2013; Oberoi et al., 2011), the yeast Tup1
52 (Matsumura et al., 2012), and its homologs Drosophila Groucho (Gro) and mammalian
53 transducing-like enhancer (TLE) (Agarwal et al., 2015).

54 In plants, TOPLESS (TPL), TOPLESS-RELATED (TPR1-4), LEUNIG (LUG) and its
55 homolog (LUH), High Expression of Osmotically responsive genes 15 (HOS15) all act as
56 Gro/TLE-type corepressors (Causier et al., 2012; Lee and Golz, 2012; Liu and Karmarkar, 2008;
57 Long et al., 2006; Zhu et al., 2008). Defects in the TPL family have been linked to aberrant stem
58 cell homeostasis (Busch et al., 2010), organ development (Gonzalez et al., 2015), and hormone
59 signaling (Causier et al., 2012; Kagale et al., 2010), especially the plant hormone auxin (Long et
60 al., 2006). Plant corepressors share a general structure, where at the N-terminus a LIS1
61 homology (LisH) domain contributes to protein dimerization (Delto et al., 2015; Kim et al., 2004).
62 At the C-terminus, WD40 repeats form beta-propeller structures that are involved in protein-
63 protein interactions (Collins et al., 2019; Liu et al., 2019). In TPL family corepressors, the LisH is
64 followed by a C-terminal to LisH (CTLH) domain that binds transcriptional repressors through an
65 Ethylene-responsive element binding factor-associated Amphiphilic Repression (EAR) motif
66 found in partner proteins (Causier et al., 2012; Kagale et al., 2010). The N-terminal domain also
67 contains a CT11-RanBPM (CRA) domain, which provides a second TPL dimerization interface
68 and stabilizes the LisH domain (Ke et al., 2015; Martin-Arevalillo et al., 2017). While there is
69 speculation that the beta-propellers may control protein interaction with other repressive
70 machinery, it is well-established that they bind to the non-EAR TPL recruitment motifs found in
71 transcriptional regulators (RLFGV- and DLN-type motifs, (Liu et al., 2019)).

72 We have previously demonstrated the recapitulation of the auxin response pathway in
73 *Saccharomyces cerevisiae* (yeast) by porting individual components of the *Arabidopsis* auxin
74 nuclear response (Pierre-Jerome et al., 2014). In this *Arabidopsis thaliana* Auxin Response
75 Circuit in *Saccharomyces cerevisiae* (*At*ARC$^{Sc}$), an auxin responsive transcription factor (ARF)
76 binds to a promoter driving a fluorescent reporter. In the absence of auxin, the ARF protein
77 activity is repressed by interaction with a full-length Aux/IAA protein fused to the N-terminal
78 domain of TPL. Upon the addition of auxin, the TPL-IAA fusion protein is targeted for
79 degradation through interaction with a member of the Auxin Signaling F-box protein family (TIR1
80 or AFB2), and releases the transcriptional repression of the fluorescent reporter. Reporter
81 activation can be quantified after auxin addition by microscopy or flow cytometry (Pierre-Jerome
82 et al., 2014). In the original build and characterization of *At*ARC$^{Sc}$, it was noted that the two N-
83 terminal truncations of TPL (N100 or N300) behave differently (Pierre-Jerome et al., 2014).
84 While both truncations are able to repress the function of a transcriptional activator fused to an
85 Aux/IAA, only the TPLN100 fusion shows alleviation of repression after auxin addition. TPLN300
86 fusions to Aux/IAAs maintain strong durable repression even under high concentrations of
87 auxin. This disparity is not due to differential rates of protein degradation, as both proteins
88 appear to be turned over with equal efficiency after auxin addition (Pierre-Jerome et al., 2014).
89 Structures of the N-terminal domains of TPL rice homolog OsTPR2 (Ke et al., 2015) and
90 the *Arabidopsis* TPL (Martin-Arevalillo et al., 2017) have recently been solved. These structures
91 reveal high conservation of protein folds in the N-terminus, as well as the residues that
92 coordinate formation of homotetramers (Figure 1A). Several lines of evidence suggest that the
93 multimeric TPL modulates repression potential. First, the dominant TPL mutant *tpl-1* altered a
94 single amino acid in the ninth helix of the TPL-N terminus (N176H) that induces aggregation of
95 TPL and its homologs (TPR1-4), reducing total activity (Long et al., 2006; Ma et al., 2017).
96 Second, TPL recruitment motifs found in the rice strigolactone signaling repressor D53 induce
97 higher-order oligomerization of the TPL N-terminus, which increases histone binding and
98 transcriptional repression (Ma et al., 2017). Third, structural studies of *Arabidopsis* TPL
99 demonstrated interdependency of the TPL tetramer formation and Aux/IAA binding (Martin-
100 Arevalillo et al., 2017). One contrary piece of evidence is the strong repressive activity of the
101 TPL N100 construct which lacks the majority of the CRA domain ((Martin-Arevalillo et al., 2017),
102 Figure 1A) and is unlikely able to form tetramers.

103 The conservation of TPL's repressive function in yeast suggests that the protein partners
104 that enact the repression are conserved across eukaryotes. Consistent with this speculation, the
105 series of alpha-helices that form the N-terminal portion of TPL is highly reminiscent of naturally-
106 occurring truncated forms of mammalian TLE (Gasperowicz and Otto, 2005), such as Amino-
107 terminal Enhancer of Split (AES) (Zhang et al., 2010), the Groucho ortholog LSY-22 (Flowers et
108 al., 2010), and the unrelated mouse repressor protein MXI1 (Schreiber-Agus et al., 1995).
109 Gro/TLE family members are generally considered to repress by recruiting histone deacetylases
110 to control chromatin compaction and availability for transcription (Chen and Courey, 2000; Long
111 et al., 2006). An alternative hypothesis has been described for Tup1 in yeast, where Tup1
112 blocks the recruitment of RNA Polymerase II (Pol-II) (Wong and Struhl, 2011), possibly through
113 contacts with Mediator complex subunits Med21 or Med3 (Gromöller and Lehming, 2000;
114 Papamichos-Chronakis et al., 2000). However, like many of these family members, multiple
115 repression mechanisms have been described for TPL at different genetic loci. For example, TPL
116 has been found to recruit the repressive CDK8 Mediator complex (Ito et al., 2016), chromatin
117 remodeling enzymes such as Histone Deacetylase 19 (HD19) (Long et al., 2006) and directly
118 bind to histone proteins (Ma et al., 2017).
119 Here, we leveraged the power of yeast genetics to interrogate the mechanism of TPL
120 repression. Using *At*ARC$^{Sc}$, we discovered that the N-terminal domain of TPL contains two
121 distinct repression domains that can act independently. We mapped the first, weaker repression
122 domain to the first 18 amino acids of the LisH domain (Helix 1), and the second, more potent
123 domain to Helix 8 which falls within the CRA domain. Full repression by Helix 8 required direct
124 interaction with the Mediator complex, through interactions with Med21 and Med10. This
125 interaction required the same Med21 residues that control transcriptional activation of Tup1-
126 regulated genes in yeast. In addition, we found that multimerization of TPL was not required for
127 repression in yeast or in plants. Our yeast results were validated with plant assays, and
128 extended to include evidence that interaction with the middle domain of Mediator was required
129 for TPL repression of the auxin genes governing lateral root development. Our findings point to
130 a conserved functional connection between Tup1/TPL corepressors and the Mediator complex
131 that together create a repressed state with the capacity for rapid activation.
132
133 **Results**

134 To understand how TPL represses transcription, we first sought to localize repressive activity
135 within the protein. In the *At*ARC$^{Sc}$, the extent of auxin-induced turnover of TPLN100 and
136 TPLN300 fusions appear similar, although neither are completely degraded (Pierre-Jerome et
137 al., 2014). One interpretation is that auxin addition increases the sensitivity of the assay to
138 detect subtle differences in the strength of repressive activity of each fusion protein by reducing
139 its relative concentration. In this light, we would argue that TPLN300 is a stronger repressor
140 than TPLN100. To further exploit this synthetic repression assay, we began by generating a
141 deletion series of the N-terminus guided by the available structural information (Figure 1A-B,
142 (Ke et al., 2015; Martin-Arevalillo et al., 2017)). We started with a TPLN188-IAA3 fusion protein
143 construct, which behaves identically to TPLN300 (Figure 1B, (Pierre-Jerome et al., 2014)), and
144 subsequently deleted each alpha helical domain starting with Helix 9 (constructs are named in
145 the format Helix x – Helix y or Hx-Hy). We found that Helix 8 was required for the maximum
146 level of repression activity and for the maintenance of repression after auxin addition (Figure
147 1C). All constructs lacking Helix 8 retained the ability to repress transcription, but this repression
148 was lifted in the presence of auxin (Figure 1C) as had been observed for the original TPLN100
149 construct (Pierre-Jerome et al., 2014). Further deletions revealed that including only the 18
150 amino acids of Helix 1 was sufficient to confer repression (H1, Figure 1D). To test whether Helix
151 8 activity depended on Helix 1, we tested an additional construct consisting solely of Helix 3
152 through Helix 9 (H3-H9, Figure 1D). This construct was also able to repress ARF activity, thus
153 demonstrating that both Helix 1 (LisH) and Helix 8 (CRA) can act independently of one another
154 (Figure 1D). To identify the minimal domain needed for Helix 8-based repression, we generated
155 new deletions (Figure 1B,E-F). Helix 8 and the following linker were not sufficient for repression
156 (Figure 1E), and removal of Helix 9 or of the linker between Helix 8 and Helix 9 slightly
157 increased sensitivity to auxin compared to TPLN188 (H1-H8Δ8L, Figure 1F). A deletion that
158 removed both the LisH and Helix 8 repression domains (H3-H7) was only able to weakly
159 repress reporter expression (Figure 1F). Together, these results demonstrate that Helix 1 and
160 Helix 8 could act as repression domains, and that the linker between Helix 8 and Helix 9 (which
161 folds over Helix 1) was required for repression following addition of auxin. Helix 1 alone in the
162 LisH domain was sufficient to act on its own as a modular repression domain. The repressive
163 activity of Helix 8 was only functional in the context of the larger Helix 3-Helix 8 truncation that
164 carries the CTLH domain and a portion of the CRA domain.
165

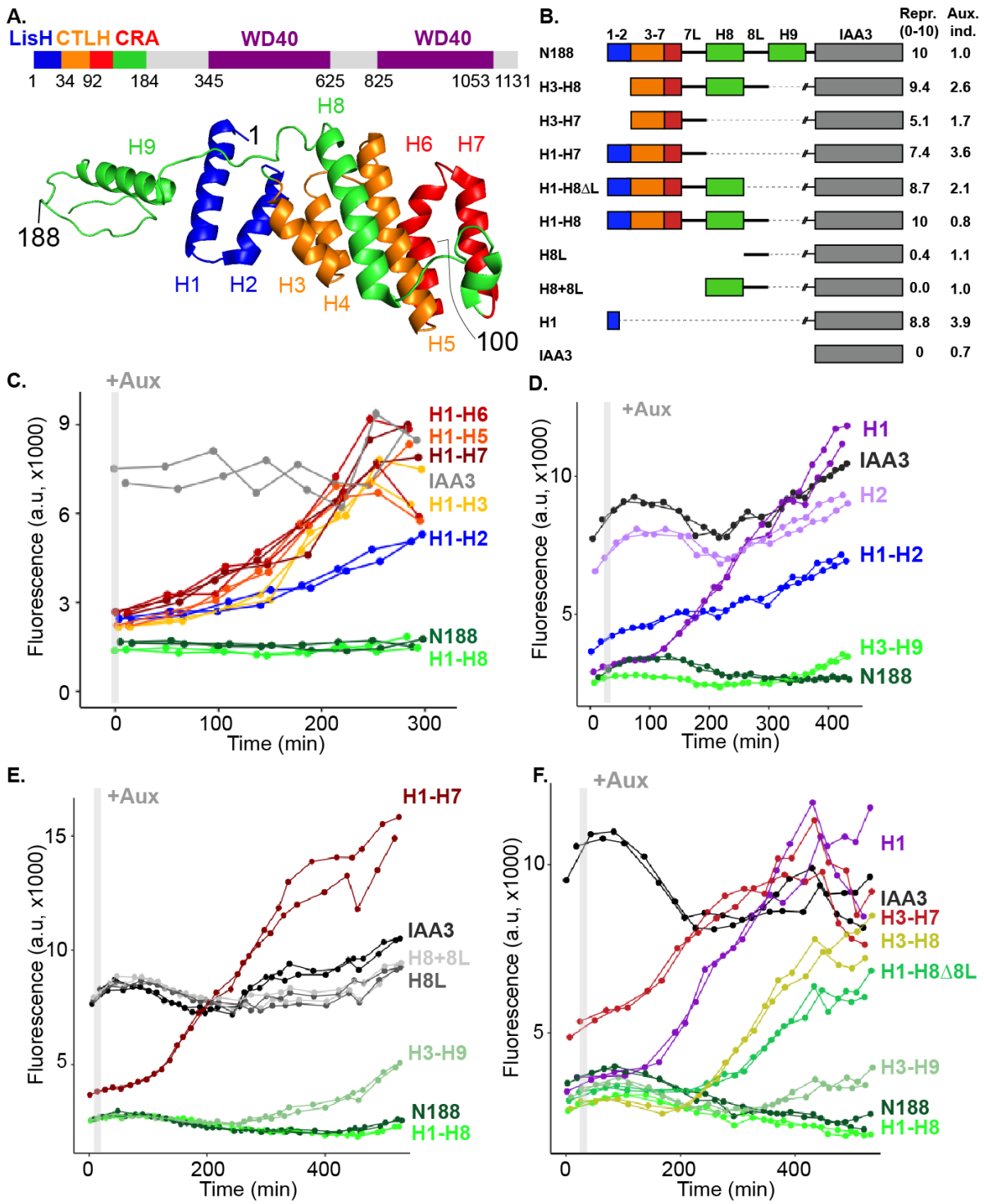


**Figure 1. The N-terminal domain of TPL contains two independent repression domains.** **A.** TPL domains are LisH (LIS1 homology motif, blue), CTLH (C-terminal LisH motif, orange), CRA (CT11-RanBPM, red - dimerization and green - foldback), and two WD40, beta-propeller motifs (purple). N-terminal domains are indicated on the solved structure of the first 202 amino acids ((Martin-Arevalillo et al., 2017), 5NQS). The termini of the TPL-N100 truncation used in

171 the original ARC$^{Sc}$ studies is indicated. **B.** Diagram indicating the structure of constructs
172 analyzed in experiments shown in subsequent panels. Repression Index (Rep.) is a scaled
173 measure of repression strength with 0 set to the level of repression observed with IAA3 and 10
174 set to the level of repression by TPLN188-IAA3. Auxin induction level (Aux.) indicates the fold
175 change difference between reporter expression before auxin addition (time zero) and at the end
176 of an experiment (~500 minutes) **C-F.** Helix 1 and the CRA domain (Helix 3-Helix 8) can act
177 independently to repress transcription. Each panel represents two independent time course flow
178 cytometry experiments of the TPL helices indicated, all fused to IAA3. Every point represents
179 the average fluorescence of 5-10,000 individually measured yeast cells (a.u. - arbitrary units).
180 Auxin (IAA-10μM) was added at the indicated time (gray bar, + Aux).
181
182 To determine which of the many known or predicted TPL-binding partners could mediate
183 the repression activity of Helix1 and Helix8, we identified known interactors with either TPL or
184 other Gro/TLE co-repressors, and then introduced the *Arabidopsis* homologs of these genes
185 into the cytoSUS system (Asseck and Grefen, 2018). We chose the cytoSUS system as it would
186 remove the interaction between target proteins to the cytoplasm, as we observed that anchoring
187 the TPL N-terminus had the capacity to repress transcriptional activation of both our synthetic
188 auxin reporter and the activation of yeast two hybrid prototrophy reporters (Figure 1,
189 Supplemental Figure 1A). Putative direct interactors include histone deacetylases (HDACs -
190 AtHDAC9, AtHDAC6, (Long et al., 2006)), Histone proteins (Histone H3, Histone H4, (Ma et al.,
191 2017)), and the Mediator components MED13 (AtMED13, (Ito et al., 2016)) and MED21, which
192 has been demonstrated to interact with Tup1, the yeast homolog of TPL (Gromöller and
193 Lehming, 2000). We did not observe any interactions between TPL-N188 and the HDACs HDA6
194 and HDA9; the histone protein AtHIS4; or the Mediator subunit AtMED13 (Figure 2A,
195 Supplemental Figure 1B). HDAC interaction with TPL has been previously hypothesized to
196 occur through indirect interactions with partner proteins (Krogan et al., 2012), however direct
197 interactions with histones and MED13 have been detected (Ito et al., 2016; Ma et al., 2017). The
198 absence of interaction between TPL-N188 and these proteins may be due to differences
199 between methods, or interaction interfaces in the C-terminal WD40 repeats.
200 Strong interaction was detected between TPL-N188 and AtMED21, a component of the
201 Mediator middle domain (Figure 2A). MED21 is one of the most highly conserved Mediator
202 subunits (Bourbon, 2008), and has a particularly highly conserved N-terminus (Supplemental

203 Figure 2A,C-E). In yeast, Tup1 interacts with the first 31 amino acids of ScMed21, with the first
204 seven amino acids being absolutely required (Gromöller and Lehming, 2000). We observed that
205 the equivalent truncation of AtMED21 (AtMED21-N31) was sufficient for interaction with TPL-
206 N188 (Figure 2A). We next created truncations of the N-terminal domain of AtMED21 to closely
207 match those that had been made in yeast (Figure 2B, Supplemental Figure 2B) where deletion
208 of the first five amino acids of ScMed21 (ScΔ5Med21) severely reduce the ability of the
209 Mediator complex to co-purify with Pol-II and CDK8 kinase complex (Sato et al., 2016).
210 Interaction between TPLN188 and AtMED21 similarly required the first five amino acids of
211 AtMED21 (Figure 2B), and this truncation did not significantly impact protein levels (Figure 2B).
212 We used cytoSUS screening to ask whether TPL-N188 interacted with other middle
213 domain Mediator components, and identified an interaction with AtMED10B (Figure 2C). There
214 are two MED10 isoforms in *Arabidopsis*; AtMED10A and AtMED10B with 76.5% amino acid
215 identity between isoforms, and *AtMED10B* is nearly always expressed at a higher level than
216 *AtMED10A* (Klepikova et al., 2016). Consistent with the cytoSUS results, TPLN188 was able to
217 pull down both AtMED21 and AtMED10B from yeast extracts (Figure 2D). AtMED21 interaction
218 was specific to the Helix8-based repression domain, as it interacted with TPLH3-H9 (Figure 2E),
219 and not TPLH1-H5 (Supplemental Figure 1C). A manual juxtaposition of the yeast Mediator
220 structure with the *Arabidopsis* TPL N-terminal structure shows that Helix 8 and 9 of TPL face
221 away from the tetramer, and are therefore optimally placed to interact with Mediator
222 components (Figure 2F).

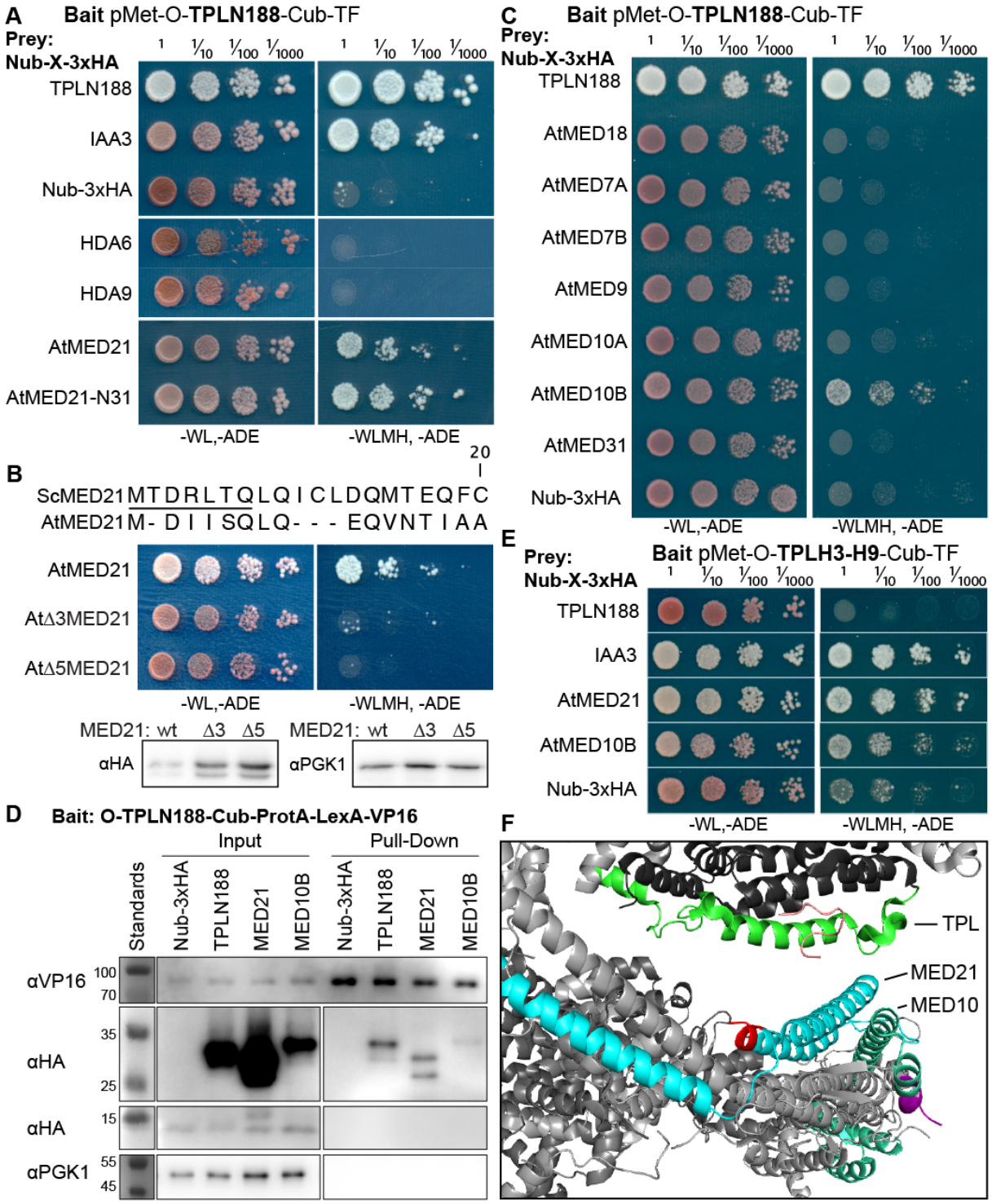


**Figure 2. The Helix 8 repression domain of TPL directly interacts with AtMED21 and AtMED10B. A-C,E.** cytoSUS assays with candidate interacting proteins. Nub-3xHA is the N-terminal fragment of Ubiquitin expressed with no fusion protein and is used as a negative control. Each prey protein is from *Arabidopsis*. -WL, -ADE - dropout lacking Trp, Leu and Ade

227 (growth control), -WLMH, -ADE – dropout lacking Trp, Leu, His, Met, and Ade (selective media).
228 **B**. Alignments of the *Arabidopsis* (At) and *Saccharomyces* (Sc) MED21 proteins are shown
229 above cytoSUS assays with the same bait shown in (**A)**. Western blots below the colonies
230 indicated that AtMED21 N-terminal Δ3 and Δ5 are well expressed in assay conditions. **C.**
231 cytoSUS assays with selected Mediator proteins in the middle module. **D.** The TPL-ProteinA-TF
232 fusion protein can pull down TPL, AtMED21 and AtMED10B from yeast extracts using IgG-
233 beads. Detection of the VP16 transcriptional activator demonstrates enrichment of the fusion
234 protein (αVP16). Each prey protein is detected via the 3xHA tag (αHA), and efficacy of
235 purification was judged by PGK1 depletion (αPGK1). **E.** A TPL-N truncation lacking the LisH
236 domain (TPLH2-H9) could still interact with the AtMED21-N31 truncation. This bait construct
237 interacted with IAA3, but only minimally with the negative control (free Nub-3xHA). **F.** Yeast
238 Mediator (bottom, 5N9J) and AtTPL (top, 5NQV) manually docked to compare relative domain
239 sizes and feasibility of a TPL-MED21-MED10B interaction. TPL Helix 8-9 is colored green.
240 MED21 is colored aqua, with the N-terminus colored red, and the EAR peptide in orange.
241 MED10 is colored teal, with the C-terminus colored purple.
242
243 To pinpoint which residues of Helix3-9 could coordinate repression through interaction
244 with MED21, we identified likely solution-facing amino acids from Helix 8, as this helix had the
245 greatest impact on repression strength (Figure 1C). We hypothesized that these amino acids
246 were not involved in stabilizing the hydrophobic interactions between intra-TPL helical domains
247 and might be available to interact with partner proteins. In the context of H3-H8-IAA3, eight
248 amino acids in Helix 8 were mutated to alanine (Figure 3A, light green residues). Repression
249 activity was assessed in the absence (Figure 3B) or presence (Figure 3C) of auxin. No single
250 amino acid was essential for repression (Figure 3B). Two mutations (R140A and K148A) slightly
251 increased baseline expression of the reporter (Figure 2B-C). All mutations, except E152A that
252 behaved similarly to controls, altered the stability of repression after auxin addition, either by
253 increasing (S138A,V145A, E146A, K149A) or decreasing (I142A) the final fluorescence level
254 (Figure 2C). Mutating E146 and K149 also increased the speed with which the reporter
255 responded to auxin (Figure 2C), suggesting that these two neighboring residues could be a
256 critical point of contact with co-repressive machinery. S138A had a small increase in auxin
257 sensitivity, while I142 reduced auxin sensitivity (Figure 2E). TPL/TPR corepressors are recruited
258 to transcription factors through an Ethylene-responsive element binding factor-associated

259 Amphiphilic Repression (EAR) motif (Causier et al., 2012; Kagale et al., 2010), which binds to
260 the TPL in a pocket adjacent to Helix 8 (Ke et al., 2015; Martin-Arevalillo et al., 2017). While
261 these two residues (S138A, I142) do not contact the conserved leucine residues of the EAR
262 motif (LxLxL), in the AtTPL structure, the C-terminal portion of the IAA27 EAR domain makes
263 contact with these residues (Martin-Arevalillo et al., 2017). As we are using a TPL-IAA fusion
264 protein, repression does not depend on EAR-TPL interaction, therefore making it difficult to fully
265 assess any role this interaction normally plays in recruiting repression machinery.
266 We tested whether the residues in Helix 8 that were required for repression (V145,
267 E146, K148, K149, Figure 3A-C) were also required for interaction with AtMED21. Single
268 alanine mutations of these four amino acids in the context of TPLN188 significantly reduced
269 interaction with AtMED21, while the quadruple mutation (here called Quad$^{AAAA}$) completely
270 abrogated AtMED21 binding (Figure 3D). These mutations had little effect on interaction with
271 AtMED10B (Supplemental Figure 1D). Additionally, we observed that most of these single
272 mutations decreased binding between TPL and IAA3, consistent with their position along the
273 EAR binding pocket (Figure 3D). When tested in the *At*ARC$^{Sc}$, TPLN188-Quad$^{AAAA}$ resembled
274 the repressive activity of wild-type N188 (red and black, Figure 3E), consistent with the
275 observation that Helix 1 is present in this construct and is sufficient for repression (Figure 1D).
276 Introduction of Quad$^{AAAA}$ mutations into the Helix 3 through Helix 8 context (H3-H8-Quad$^{AAAA}$)
277 largely phenocopied a Helix 3 through Helix 7 truncation (H3-H7, Figure 1F) with a drastically
278 reduced repression strength and rapid alleviation of repression by auxin addition (yellow and
279 pink, Figure 4E). Residual repression in H3-H7 likely comes from binding to MED10B, which
280 binds outside amino acids 145-149 (Supplemental Figure 1D). These results indicate that the
281 CRA domain (H3-H8) requires contact with MED21 to repress, and that this is independent of
282 the repression via Helix 1.
283

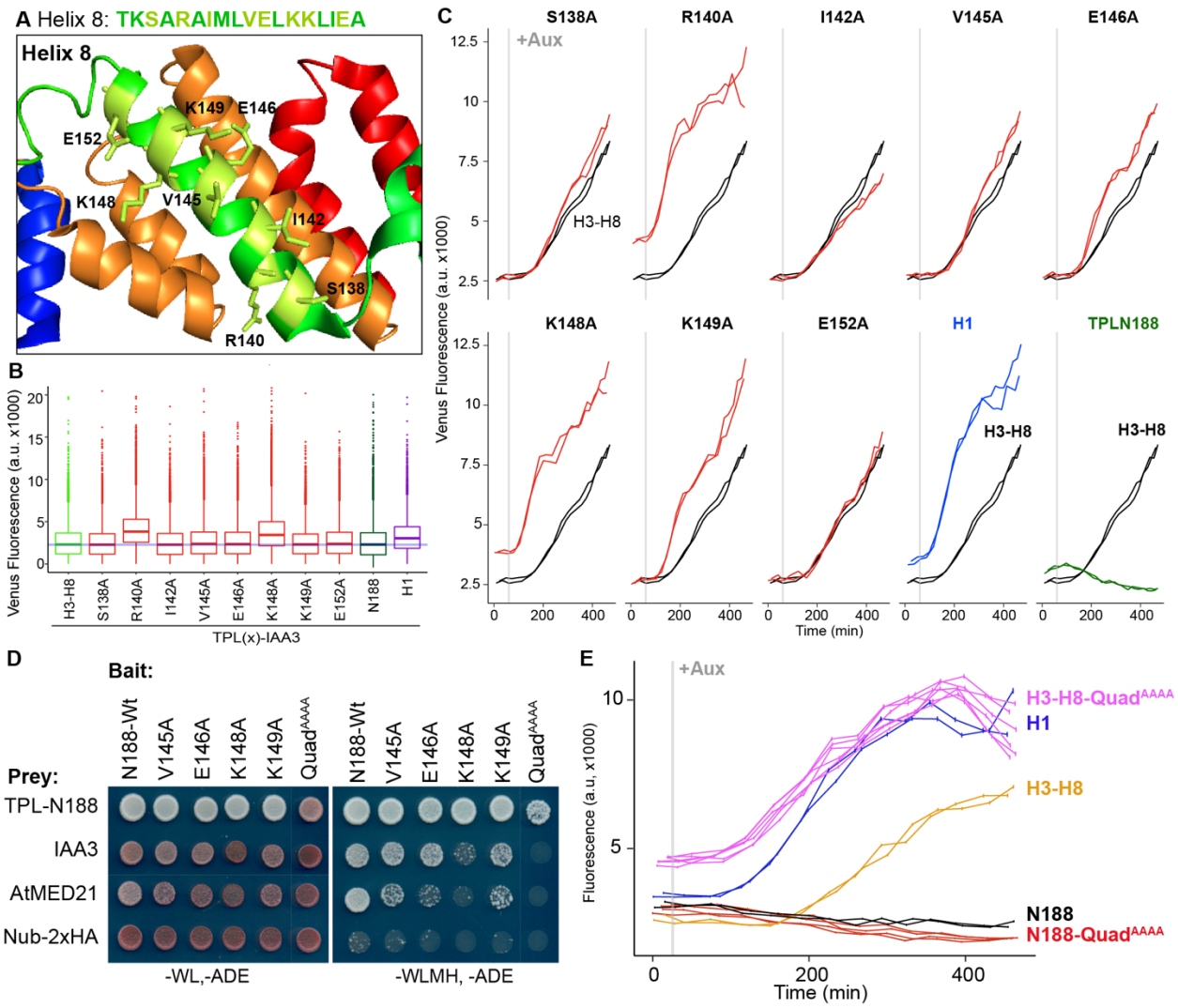


**Figure 3. Identification of critical residues within Helix 8 repression domain. A.** Sequence and structure of Helix 8 (5NQS). Helix 8 is colored green, and amino acids chosen for mutation are highlighted in light green in both the sequence and the structure. **B.** Repression activity of indicated single and double alanine mutations. **C.** Time course flow cytometry of selected mutations of Helix 8 following auxin addition. TPLH3-8-IAA3 fusion proteins (black) were compared to indicated single mutations to alanine (red). Controls - Helix 1 (H1 – blue), and TPLN188 (dark green). **D.** A series of alanine mutations (V145A, E146A, K148A, K149A, and the quadruple mutant Quad$^{AAAA}$ chosen from Figure 2D-F) were introduced into the TPL-N188 bait construct and tested for interaction with wild-type TPL-N188, IAA3 and AtMED21. Each single alanine mutation reduces TPL interaction with AtMED21, while the quad mutation abrogated interaction. These mutations also reduced the binding strength of TPLN with IAA3. **E.** The Helix 8 Quad$^{AAAA}$ mutation was introduced into the TPLN188-IAA3 and TPLH3-8-IAA3

296 fusion proteins and compared to wild type N188 in time course flow cytometry. For all cytometry
297 experiments, the indicated TPL construct is fused to IAA3. Every point represents the average
298 fluorescence of 5-10,000 individually measured yeast cells (a.u. - arbitrary units). Auxin (IAA-
299 10μM) was added at the indicated time (gray bar, + Aux). At least two independent experiments
300 are shown for each construct.
301
302 The TPL N-terminus (N188) interacted with at least two components of the Mediator
303 complex, AtMED21 and AtMED10B, and interaction between residues in Helix 8 (V145, E146,
304 K148, K149) were necessary for repression (Figure 3). These results suggest that the Mediator
305 complex is required for the TPL N-terminal domain to control repression (Figure 4A). To
306 determine whether a protein-protein interaction is required for corepressor function, it is critical
307 to demonstrate that reciprocal loss of function mutations activate repressed genes. In the case
308 of Tup1, a standard approach has been to test deletion mutations of Tup1-interacting proteins to
309 determine whether their interaction represents a true repression modality on the target gene
310 (Gromöller and Lehming, 2000; Lee et al., 2000; Zhang and Reese, 2004). We sought to test
311 whether loss of function in the Mediator complex would result in activation of the TPL-repressed
312 reporter in the *At*ARC$^{Sc}$. However, Mediator loss of function mutants can be lethal or exhibit
313 drastic physiological phenotypes (Biddick and Young, 2005). Instead, we combined the Anchor
314 Away system for rapid, chemically conditional protein depletion (Haruki et al., 2008) with the
315 auxin response circuit (Figure 4B).
316 *At*ARC$^{Sc}$ integrates components at four genomic locations using prototrophic markers
317 that are not compatible with those needed for Anchor Away. To overcome this limitation, we re-
318 recreated the entire ARC on a single plasmid (SLARC) using the Versatile Genetic Assembly
319 System (VEGAS, (Mitchell et al., 2015)). SLARC behaved with similar dynamics to the original
320 *At*ARC$^{Sc}$ on both solid and liquid growth conditions (Supplemental Figure 3A-C). As a first test of
321 the Anchor Away system with SLARC, we fused Tup1 and its partner protein Cyc8 to two copies
322 of the FKBP12-rapamycin-binding (FRB) domain of human mTOR (Haruki et al., 2008).
323 Rapamycin treatment of strains targeting either of these proteins caused no release of
324 repression, providing confirmation that the ARC acts orthogonally to the yeast corepressor
325 (Supplemental Figure 3D).
326 To test whether Mediator proteins or specific modules were required for TPL repression
327 we introduced the fully repressed SLARC plasmid containing TPLN188 (SLARC$^{N188}$) into a

328 library of Anchor Away yeast strains that allow specific depletion of Mediator components (see
329 Figure 4A-B) developed in (Haruki et al., 2008; Petrenko et al., 2017). Upon nuclear depletion of
330 the target genes we saw a striking activation of the auxin reporter when Mediator components
331 from the Tail, Head, and Middle domains were depleted (Figure 4C-E). We observed a less
332 pronounced activation upon depletion of CDK8 (Figure 4F), suggesting that this module plays
333 an ancillary role compared to the core Mediator complex. It is critical to note that Anchor Away
334 of components that are absolutely required for transcriptional activation will show no activation,
335 such as the Tail triple Anchor Away (17,3,15 - Figure 4C) or the RNA Polymerase II (Pol II)
336 Anchor Away (Rpb1 – Figure 4G). These observations support the interpretation that the entire
337 Mediator core (Tail, Head, Middle) is required for robust repression by the TPL N terminus,
338 which is recruited to the middle domain by MED10 and MED21.
339 Because we have pinpointed TPL N-terminal repression and protein interaction to the
340 specific region of AtMED21 we chose to focus in on this region in the yeast Med21 protein.
341 Deletion of the first 7 amino acids of ScMed21 (Δ7Med21) partially releases genes that are
342 normally repressed by Tup1 into a transcriptionally active state (Gromöller and Lehming, 2000).
343 We hypothesized that TPL repression would also be partially alleviated by such a deletion.
344 ScMed21 is an essential gene, and yeast carrying deletions like Δ7Med21 grow more slowly
345 than the wild type (Gromöller and Lehming, 2000; Hallberg et al., 2006), which itself alters
346 expression levels of reporters. In fact, even a Δ5Med21 yeast mutant has been demonstrated to
347 alter Mediator assembly as the first 5 amino acids of ScMed21 are required for binding of Pol II
348 and the CDK8 kinase module to the Mediator core (Hallberg et al., 2006; Sato et al., 2016).
349 We introduced SLARCs with different TPL constructs into strains where ScMed21 wild-
350 type or N-terminal deletions were stably expressed and targets of Anchor Away. Strains
351 expressing ScMed21 with or without FRB fusions behaved similarly (Figure 4H, Supplemental
352 Figure 3E-F). We compared the transcriptional output of the fully repressed SLARC$^{N188}$ in
353 MED21 N-terminal mutants lacking the first three, five or seven amino acids. We observed that
354 all three deletions significantly increased the expression of the reporter in SLARC$^{N188}$, while no
355 mutation increased the SLARC's sensitivity to auxin (Figure 4H, Supplemental Figure 3E-F). As
356 Δ7ScMed21 did not increase reporter expression when compared to Δ5ScMed21 yet did have a
357 noticeable impact on growth, we did not use it in further analyses. Deletions of ScMed21 N-
358 terminal residues had no effect on repression in SLARC$^{H1-H5}$ but they do impair auxin responsive
359 transcriptional activation (Figure 4I), consistent with the role of this region in promoting Pol-II

360 recruitment (Sato et al., 2016). The fully repressed SLARC$^{N188}$ in Δ3ScMed21 or Δ5ScMed21
361 mutants showed elevated transcription of the reporter and when depleted demonstrate an
362 increase in reporter activity (Figure 4J), indicating that there is still residual TPLN188-Mediator
363 interaction taking place. Conversion of the first five amino acids of ScMed21 to the
364 corresponding sequence from AtMED21 resulted in an identical repression profile
365 (Supplemental Figure 4E), and had no effect on yeast growth or viability (Supplemental Figure
366 4F), further highlighting the conservation of this repression mechanism between the two
367 organisms.
368 The stably expressed N-terminal deletions of ScMed21 likely alter the expression of
369 multiple yeast genes, and this state change could confound our interpretations of the
370 importance of ScMed21 on TPL repression. To minimize the off-target impact of ScMed21
371 deletions, we introduced estradiol inducible versions of ScMed21 (iScMed21) into the Anchor
372 Away SLARC$^{N188}$ strains (Figure 4B, (McIsaac et al., 2013)). The combination of all three
373 synthetic systems made it possible to rapidly deplete the wild type ScMed21-FRB from the
374 nucleus while simultaneously inducing ScMed21 variants and visualizing the impact on a single
375 auxin-regulated locus. Depletion of nuclear ScMed21 by Rapamycin increased levels of the
376 reporter in all genotypes examined (Figure 4J) while also increasing cell size even in short time-
377 courses, consistent with its essential role in many core pathways (Supplemental Figure 4A,
378 (Gromöller and Lehming, 2000)). When wild-type iScMed21 was induced, there was a rescue of
379 both phenotypes (Figure 4K, black), whereas induction of either Δ3 and Δ5 variants
380 recapitulated the reporter activation seen in the stably expressed mutant versions (Figure 4K,
381 green and blue, Supplemental Figure 4B). iΔ3Med21 was induced and accumulated at a
382 comparable level to wild type Med21, while Δ5 appears to be less stable (Figure 4L-M). In these
383 short time courses, we did not observe the cell size increases observed in the Rapamycin
384 treatments (populations were evenly distributed around a single mean, suggesting we were
385 observing the immediate effects of the Med21 deletions (Supplemental Figure 4C-D)).

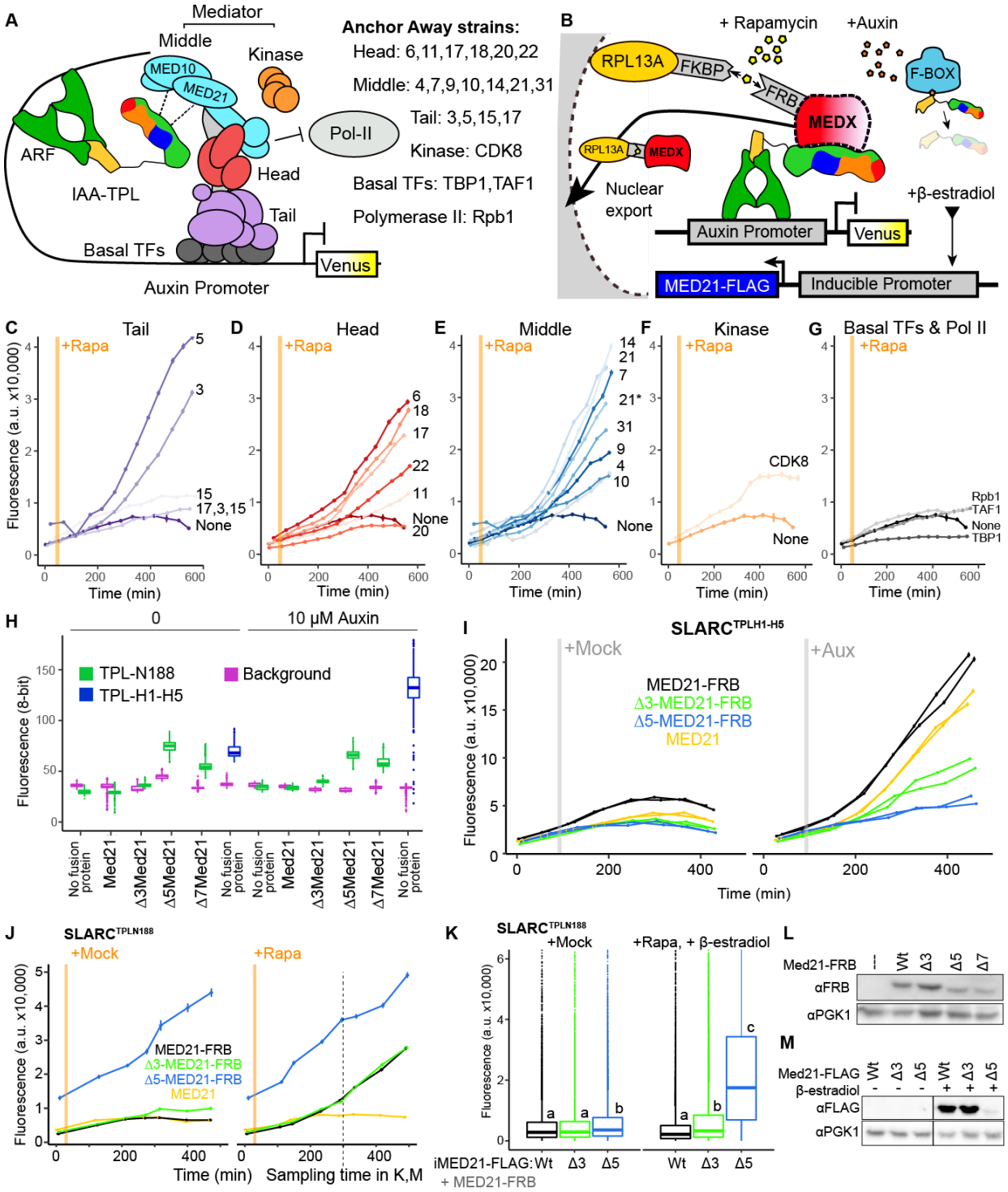


386 **Figure 4. Repression by TPL requires interaction with the N-terminus of MED21.**

387 **A.** Model of the proposed interaction between the TPL N-terminus with Mediator, where TPL

388 interaction with Mediator 21 and 10 inhibit the recruitment of Pol-II. Proteins in this complex that

389 were tested by Anchor Away are listed on the right. **B.** Schematic of *At*ARC$^{Sc}$ combined with

390 methods for inducible expression and nuclear depletion of MED21. In Anchor Away, the yeast
391 ribosomal protein 13A (RPL13A) is fused to the rapamycin binding protein FKBP. Addition of
392 Rapamycin induces dimerization between FKBP and any target protein fused to FRB, resulting
393 in removal of the target protein from the nucleus. For these experiments, *At*ARC$^{Sc}$ was
394 assembled into a single plasmid (SLARC) rather than being integrated into separate genomic
395 loci (Figure 4 – Figure Supplement 1). Estradiol-inducible ScMed21 (iMed21) made it possible
396 to replace wild-type MED21 with targeted deletions or mutations. **C-G.** Time-course flow
397 cytometry analysis of SLARC$^{N188}$ in Mediator Anchor Away yeast strains with Rapamycin
398 (orange bar, + Rapa). Two Med21 strains were compared in the Middle domain (E), 21
399 (generated in this study) and 21* (generated in (Petrenko et al., 2017)). Both 21 and 21*
400 demonstrated similar increases in reporter expression. **H.** Quantification of Venus fluorescence
401 from SLARC$^{N188}$ in wild type and N-terminal ScMed21 deletions with and without auxin. Yeast
402 was grown for 48 hours on SDO media with or without auxin and colony fluorescence was
403 quantified and plotted with the auxin responsive SLARC$^{H1-H5}$ in wild type as a reference.
404 Background - red autofluorescence was used as a reference for total cell density. **I.** Time-course
405 flow cytometry analysis of SLARC$^{H1-H5}$ in wild type and n-terminal ScMed21 deletions with and
406 without auxin. Genotypes are indicated in the colored key inset into the graph. Auxin (IAA-
407 10μM) was added at the indicated time (gray bar, + Aux). **J.** Time-course flow cytometry
408 analysis of SLARC$^{N188}$ in wild type and N-terminal ScMed21 deletions with and without
409 Rapamycin. Genotypes are indicated in the colored key inset into the graph. **K.** Rapid
410 replacement of Med21-FRB with inducible Med21-FLAG demonstrated the requirement for the
411 ScMed21 N-terminus in TPL repression. iMed21 isoforms were induced by addition of β-
412 estradiol (20μM) for 4 hours followed by Rapamycin addition. Fluorescence was quantified by
413 cytometry after 300 minutes (indicated by the dashed box in **D**). Lower case letters indicate
414 significant difference (ANOVA and Tukey HSD multiple comparison test; $p<0.001$). **L-M.** Protein
415 abundance of ScMed21 variants was tested by SDS-PAGE & western blot. For (**C-G, J**) a.u. -
416 arbitrary units. Rapamycin was added at the indicated time (orange bar, + Rapa). Every point
417 represents the average fluorescence of 5-10,000 individually measured yeast cells.
418
419 Our data indicated that truncated TPL repression domains were sufficient for interaction
420 with Mediator complex and transcriptional repression, however these truncations (i.e. TPLH3-
421 H8), are unable to form tetramers. This observation re-opened the question as to whether TPL

422 multimerization affects repression, as both the N-terminus of AtTPL and OsTPR2 adopt a
423 tetrameric form when crystallized (Figure 5A (Ke et al., 2015; Martin-Arevalillo et al., 2017)). We
424 used the cytoplasmic split ubiquitin (cytoSUS) protein-protein interaction assay (Asseck and
425 Grefen, 2018) to test this hypothesis. We observed that Helix 8 was required for strongest
426 interaction between TPL constructs (Supplemental Figure 5A), although this assessment was
427 complicated by the fact that some of the shorter constructs accumulated to significantly lower
428 levels (Supplemental Figure 5B). The weak interaction we could observe between full-length
429 TPL-N and the Helix 1 through Helix 3 construct (H1-3), indicated that the TPL LisH domain is
430 sufficient for dimerization. Therefore, while auxin-insensitive repression may require multimeric
431 TPL, this higher-order complex was not required for auxin-sensitive repression mediated by
432 Helix 1 (Figure 1C-D). In their study of the AtTPL structure, Martin-Arevalillo et al. identified a
433 triple mutation (K102S-T116A-Q117S-E122S) that abrogated the ability of the CRA domain
434 (Helix 6 and Helix 7) to form inter-TPL interactions (Martin-Arevalillo et al., 2017). As this mutant
435 form of TPL is only capable of dimerizing through its LisH domain, we refer to it here as LDimer
436 (Figure 5A). The LDimer mutations in TPLN188 retained the same auxin insensitive repression
437 auxin behavior as wild-type TPLN188 (Figure 5D), supporting the finding from the deletion
438 series.
439 To make a fully monomeric form of TPL, we introduced mutations into the dimerization
440 interface of the LisH domain in the context of LDimer. We first mutated one of a pair of
441 interacting residues (F15) to a series of amino acids (Tyrosine - Y, Alanine - A, Arginine - R, or
442 Aspartic Acid - D) in the context of either LDimer (Figure 5D), or H1-2 (Figure 5B, 5E). We
443 observed that conversion of F15 to the polar and charged aspartic acid (D) completely
444 abolished repression activity, while the polar and positively charged arginine was better
445 tolerated (Figure 5D,E). The conversion of F15 to tyrosine had no effect on LDimer (Figure 5D),
446 and only a minimal increase in auxin sensitivity in the context of H1-2 (Figure 5E). We then
447 combined LDimer-F15Y with a mutation of the coordinating residue L8 to serine with the
448 intention of stabilizing the now solvent-facing residues. The repressive behavior of this mutant
449 was indistinguishable from that of LDimer (Figure 5F). To further push the LDimer towards a
450 monomeric form, we introduced two additional mutations (S5A, E19S, Figure 5C,G). Size
451 exclusion chromatography confirmed that this combination of mutations (S5A-L8S-F15Y-E19S-
452 K102S-T116A-Q117S-E122S, hereafter called Monomer) successfully shifted the majority of the
453 protein into a monomeric state (Figure 5H); however, this shift had no observable impact on

454 repression strength before or after auxin addition (Figure 5G). To test whether these mutations
455 had a similar impact on *in vivo* TPL complexes, we introduced the LDimer and Monomer
456 mutations into the cytoSUS assay. In contrast to the *in vitro* chromatography results with purified
457 proteins, Monomer expressed in yeast retained measurable interaction with wild-type TPL,
458 LDimer or Monomer, albeit at a reduced level than what was observed between two wild type
459 TPLN188 constructs (Figure 5I). A caveat to this apparent difference between assays is that the
460 Monomer mutations led to a striking increase in protein concentration in yeast (Figure 5 – Figure
461 Supplement 1C), likely partially compensating for the decrease in affinity.
462

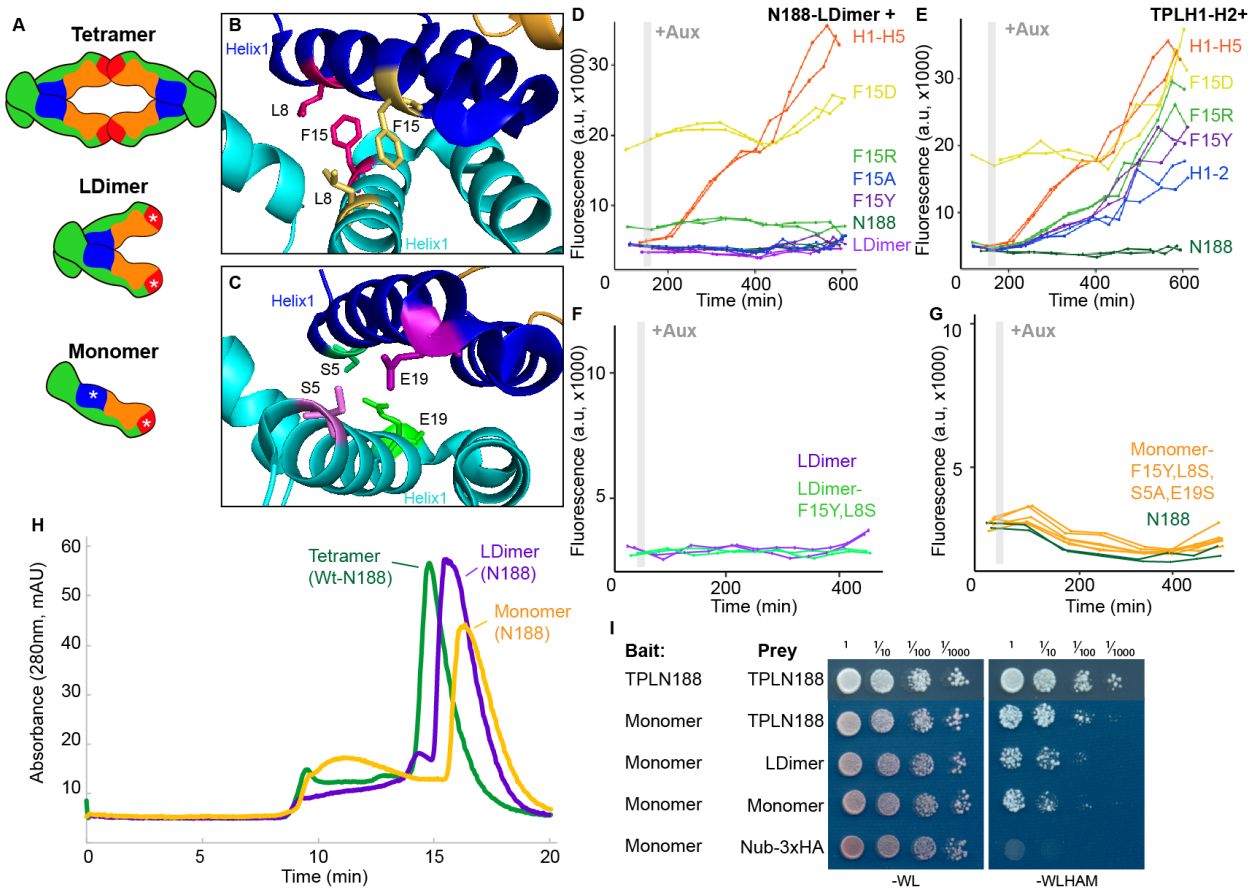


463 **Figure 5. Multimerization is not required for repression in yeast. A.** TPL can form a
464 homotetramer via the CRA (red) and LisH (blue) domains. Asterisks indicate mutations that
465 block or diminish these interactions. **B-C**. Locations of critical positions in Helix 1 are
466 highlighted for two interacting TPL monomers (shown in light and dark blue). Interacting amino
467 acids share the same color (adapted from 5NQV).

468 **D-G.** Time course flow cytometry analysis of TPLN-IAA3 fusion proteins carrying selected single
469 point mutations in N188-LDimer-IAA3 (**D**) and the TPLH1-2 truncation (**E**). The F15Y mutation
470 had little effect on repression activity for either TPL construct. Double mutations (F15Y, L8S in
471 LDimer) (**F**) or the quadruple Monomer mutations (S5A, L8S, F15Y, E19S in LDimer) (**G**)
472 showed repression activity that was indistinguishable from LDimer or wild type N188 fused to
473 IAA3. For all cytometry experiments, the indicated TPL construct is fused to IAA3. Every point
474 represents the average fluorescence of 5-10,000 individually measured yeast cells (a.u. -
475 arbitrary units). Auxin (IAA-10μM) was added at the indicated time (gray bar, + Aux). At least
476 two independent experiments are shown for each construct. **H**. Size Exclusion Chromatography
477 on TPLN188 wild type (green), LDimer (purple) and Monomer (orange) tetramerization mutants.
478 **I**. CytoSUS on TPL tetramerization mutants.
479
480 While the *At*ARC$^{Sc}$ relies on the strong conservation of the core regulatory machinery in
481 yeast and plants, there are important differences between the synthetic and native systems. For
482 example, while the TPL-N188 construct (and other variants that contain Helix 8 and the linker
483 between Helix 8 and Helix 9) repress transcription in yeast even after auxin addition, this is not
484 the case for the many auxin-regulated genes in plants. To uncover these differences, we first
485 tested for TPL and MED21 interaction using Bimolecular Fluorescence Complementation (BiFC)
486 in *Nicotiana benthamiana* (tobacco). Full-length TPL and MED21 fusions with YFP were
487 localized to the nucleus and did interact with one another by BiFC (Figure 6A). The same TPL
488 Helix 8 residues identified as necessary for a strong interaction with AtMED21 in yeast (Figure 3
489 - V145A, E146A, K148A, K149A –TPL$^{H8QuadA}$) were also important for interaction in plants
490 (Figure 6A). Similarly, the Δ5AtMED21 N-terminal truncation completely eliminated interaction
491 with full-length TPL (Figure 6A). Co-immunoprecipitation assays confirmed the AtMED21 and
492 TPL interaction (Figure 6B). We were also able to pull down MED21 and TPL using MED10B
493 from tobacco extracts, supporting our previous interaction assays from yeast (Supplemental
494 Figure 6A).
495 We next developed a UAS/GAL4-VP16-based (Brand and Perrimon, 1993) conditional,
496 quantitative repression system for plants that relied on induction of a gene encoding a TPLN-
497 IAA14 fusion protein (Figure 6A). To sensitize the output of this assay, we used a variant of
498 IAA14 with mutations in the two EAR domains (EAR$^{AAA}$) and in the degron (P306S) to block
499 interference from the endogenous TPL/TPRs or auxin-mediated degradation by the TIR1/AFBs,

500 respectively (IAA14$^{mED}$ ; Figure 6C). After prototyping the system in yeast (Supplemental Figure
501 6B), we transiently transformed constructs carrying *TPLN-IAA14$^{mED}$* variants into tobacco to test
502 repression of the well-characterized auxin response promoter DR5 (Ulmasov et al., 1997). DR5
503 was strongly induced by co-transformation with the transcriptional activator AtARF19. This
504 induction was sharply reduced if the reporter and activator were co-transformed with *UAS-*
505 *TPLN188-IAA14$^{mED}$* and *GAL4-VP16* (Figure 6D). In general, we observed strong correlation in
506 repression activity between what was observed in yeast and in tobacco. Truncations containing
507 Helix 1 (H1) or Helix 8 (H3-H9), as well as the full N-terminus (N188), repressed the DR5
508 reporter (Figure 6D). LDimer and Monomer variants retained a similarly strong repressive
509 activity in tobacco as what had been observed in yeast (Figure 6D). These results are
510 consistent with previous evidence that loss of dimerization through the CRA domain has no
511 effect on transcriptional repression of the DR5 promoter in protoplasts (Martin-Arevalillo et al.,
512 2017). We also observed congruity between yeast and plant data in that the Helix 8 quadruple
513 alanine mutation showed similar repression strength as wild type N188, possibly due to
514 presence of Helix 1 (N188$^{H8QuadA}$ - Figure 6D).
515 We were concerned that the lack of effect of the Helix 8 mutation and multimerization
516 mutants (LDimer and Monomer) on repression strength could reflect artifacts from heterologous
517 overexpression. To test the effect of these mutants in a native context, we generated transgenic
518 *Arabidopsis* lines where the UAS-TPL-IAA14$^{mED}$ constructs were activated selectively in xylem
519 pole pericycle cells, where IAA14 normally acts to regulate the initiation of lateral root primordia
520 (Figure 6E, (Laplaze et al., 2005)). Transgenic plants expressing functional TPL variants in
521 these cells should make very few if any lateral roots, phenocopying the original solitary root (*slr*)
522 mutant, which carries an auxin-resistant form of IAA14 (Fukaki et al., 2002). As expected,
523 transformants expressing either IAA14$^{mED}$ (with no TPL fusion) or TPLN188 (with no IAA14
524 fusion) had no effect on lateral root production (Figure 6F). In contrast, TPLN188 fusion
525 constructs sharply decreased lateral root density (Figure 6F). The TPLH3-H9 truncation
526 decreased lateral root density but was not as efficient as TPLN188 stressing the role of the LisH
527 in repression (Figure 6F). Both LDimer and Monomer constructs (Figure 6F) were able to
528 repress lateral root development, meaning that multimer formation is not required for TPL
529 repression of native auxin-induced genes in this context. The fusion containing the Helix 8
530 quadruple mutant demonstrated a clear loss of repression, indicating that the TPL-MED21
531 interaction is critical for repression when expressed at endogenous levels (Figure 6F).

532 AtMED21 loss-of-function mutations are embryo lethal when homozygous (Dhawan et
533 al., 2009; Supplemental Figure 6D), and plants heterozygous for *Atmed21* mutations appear
534 wild-type, including exhibiting normal lateral root density (Supplemental Figure 6E). These
535 phenotypes make testing the specific function of AtMED21interactions with TPL challenging. As
536 an alternative means to probe AtMED21 function in regulating auxin responses, we devised a
537 method to specifically repress transcription of *AtMED21* in xylem pole pericycle cells, similar to
538 the approach used for testing the function of TPL variants. To do this, we introduced a dCAS9-
539 TPLN300 synthetic repressor under the control of a UAS promoter into J0121$^{Col-0}$ along with
540 three sgRNAs complementary to the *AtMED21* promoter. If AtMED21 is required for TPL-based
541 repression, we would expect loss of AtMED21 in xylem pole pericycle cells, which would result
542 in an increase in lateral root number and length. This is indeed what we observed (Figure 6G,
543 Supplemental Figure 6F-G).
544

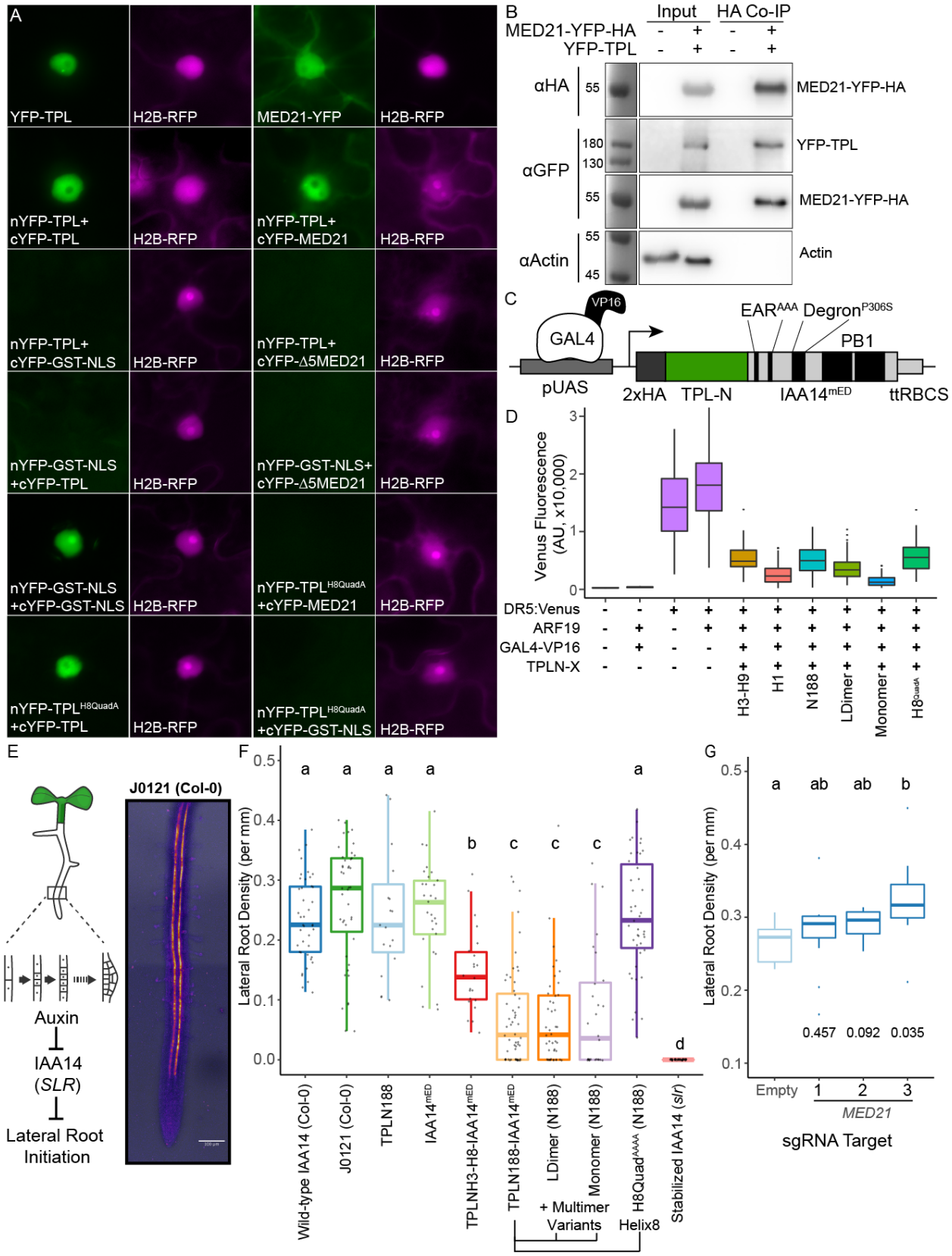
A
YFP-TPL
H2B-RFP
MED21-YFP
H2B-RFP
nYFP-TPL+ cYFP-TPL
nYFP-TPL+ cYFP-MED21
nYFP-TPL+ cYFP-GST-NLS
nYFP-TPL+ cYFP-Δ5MED21
nYFP-GST-NLS +cYFP-TPL
nYFP-GST-NLS+ cYFP-Δ5MED21
nYFP-GST-NLS +cYFP-GST-NLS
nYFP-TPLH8QuadA +cYFP-MED21
nYFP-TPLH8QuadA +cYFP-TPL
nYFP-TPLH8QuadA +cYFP-GST-NLS
B
Input
HA Co-IP
MED21-YFP-HA
YFP-TPL
αHA
αGFP
αActin
MED21-YFP-HA
YFP-TPL
Actin
C
VP16
GAL4
pUAS
EARAAA
DegronP306S
PB1
2xHA
TPL-N
IAA14mED
ttRBCS
D
Venus Fluorescence (AU, x10,000)
DR5:Venus
ARF19
GAL4-VP16
TPLN-X
H3-H9
H1
N188
LDimer
Monomer
H8QuadA
E
J0121 (Col-0)
Auxin
IAA14 (SLR)
Lateral Root Initiation
F
Lateral Root Density (per mm)
Wild-type IAA14 (Col-0)
J0121 (Col-0)
TPLN188
IAA14mED
TPLNH3-H8-IAA14mED
TPLN188-IAA14mED
LDimer (N188)
Monomer (N188)
H8QuadAAAA (N188)
Stabilized IAA14 (slr)
+ Multimer Variants
Helix8
G
Lateral Root Density (per mm)
0.457
0.092
0.035
Empty
MED21
sgRNA Target

546 **Figure 6. The TPL CRA repression domain behaves similarly in yeast and plants**
547 **A.** Bimolecular Fluorescence Complementation assay performed in tobacco. Each image is an
548 epi-fluorescent micrograph taken at identical magnification from tobacco epidermal cells at two
549 days post injection. The YFP image is colored green (left panel). p35S:H2B-RFP was used as a
550 control and is false colored magenta (right panel). **B.** Co-immunoprecipitation of MED21 and
551 TPL from tobacco leaves. MED21-YFP-HA was immunoprecipitated using anti-HA, and YFP-
552 TPL was detected using the YFP fusion. Actin was used to demonstrate that the purification had
553 removed non-specific proteins. Numbers on the left of blots indicate sizes of protein standards
554 in kilodaltons. **C.** Design of UAS-TPL-IAA14$^{mED}$ constructs. Mutation of the conserved Lysine
555 residues in the EAR domain disrupted potential interactions with endogenous TPL/TPR
556 proteins. The IAA14 degron has been mutated (P306S) to render it auxin insensitive. UAS –
557 upstream activating sequence, ttRBCS - Rubisco terminator sequence. **D.** Transient expression
558 of indicated TPL constructs in tobacco. DR5:Venus - the synthetic DR5 auxin promoter
559 (Ulmasov et al., 1997) driving Venus, ARF19 - p35S:AtARF19-1xFLAG, GAL4:VP16 -
560 pUBQ10:GAL4-VP16, TPLN-X-UAS-TPL-IAA14$^{mED}$ with various TPL truncations or mutations.
561 **E.** Auxin induced degradation of IAA14 is absolutely required for initiation of lateral root
562 development (cartoon, left). An enhancer trap line (J0121) expresses GAL4-VP16 and UAS-
563 GFP in in xylem pole pericycle cells. **F.** N-terminal domains of TPL were sufficient to repress the
564 development of lateral roots in *Arabidopsis* seedlings. The density of emerged lateral roots was
565 measured in T1 seedlings at 14 days after germination. **G.** MED21-CAS9 repressors targeted to
566 MED21 display increased lateral root densities. Lateral root density (number of lateral roots /
567 primary root length) was calculated at 10 days post germination. Numbers below boxplots are p-
568 values for pairwise comparisons with control using a Wilcoxon rank sum test. **F-G**. Lower case
569 letters indicate significant difference (ANOVA and Tukey HSD multiple comparison test;
570 $p<0.001$).
571
572
573 **Discussion**
574 A review of the current literature on corepressors gives the conflicting impressions that (a)
575 corepressor function is broadly conserved, and (b) that every organism (and perhaps even each
576 corepressor) has a distinct mode for transcriptional repression (Adams et al., 2018; Mottis et al.,
577 2013; Perissi et al., 2010; Wong and Struhl, 2011). We hoped that the *At*ARC$^{Sc}$ could facilitate a

578 resolution to this apparent contradiction by targeting repression to a single synthetic locus. We
579 focused our initial efforts on the analysis of the N-terminal portion of TPL which has multiple
580 known protein-protein interaction surfaces (Ke et al., 2015; Martin-Arevalillo et al., 2017).
581 Experiments with the *At*ARC$^{Sc}$ identified two repression domains [Helix 1 and the CRA domain
582 (Figure 1)] within the N-terminus of TPL, both of which were subsequently confirmed to repress
583 transcription in plants as well. This led us to hypothesize that they are therefore likely contact
584 points for other proteins (Figure 2). In the case of the more potent CRA domain, we were able to
585 identify two of these partners MED21 and MED10 (Figure 2). Amino acids within Helix 8 (in the
586 CRA domain) that were critical for repression activity have their R-groups oriented away from
587 the hydrophobic core of TPL structure and are required for Med21-binding and repression
588 (Figure 3). The Mediator subunit Med21 also interacts with the yeast corepressor Tup1, which
589 suggests a fundamental conservation in at least one corepressor mechanism across species.
590 Indeed, the whole core Mediator complex (Head, Middle, Tail) appears to be required for
591 repression through TPL (Figure 4). Contrary to our initial hypothesis, the monomeric form of
592 TPL was sufficient for strong repression in yeast and in plants, leaving open the question of the
593 role of higher-order TPL complex formation (Figure 5). Finally, we were able to show that the
594 TPL-MED21 interaction has functional significance for auxin response in plants (Figure 6).
595 The Mediator complex is a multi-subunit complex that connects DNA-bound transcription
596 factors and the RNA polymerase II complex (Pol-II) to coordinate gene expression (Flanagan et
597 al., 1991; Kim et al., 1994). The yeast Mediator subunits are organized into four separate
598 modules; head, middle, tail and kinase, with a strong conservation of module components in
599 plants (Dolan and Chapple, 2017; Maji et al., 2019; Malik et al., 2017; Samanta and Thakur,
600 2015). Med21 forms a heterodimer with Med7 to and interacts with Med10, among others, to
601 create the central region of the Middle region of the Mediator complex. The Med21 N-terminus
602 is centered on a flexible hinge region (Baumli et al., 2005), which is required for Pol-II
603 recruitment and CDK8 kinase module recruitment (Sato et al., 2016). The protein interaction
604 between TPL and MED21 occurs at the N-terminus of MED21, highlighting the importance of
605 this region as a signaling hub (Sato et al., 2016). Other lines of evidence support this role, as
606 this region binds the yeast homolog of TPL, Tup1 (Gromöller and Lehming, 2000) through a
607 completely different protein domain as no homology can be found between TPL Helix 8 and
608 Tup1 in any region by primary amino acid homology (i.e. BLAST).

609 Corepressors coordinate multiple mechanisms of repression through discrete protein
610 interactions, leading to robust control over eukaryotic transcription by combining repression
611 modalities. Corepressor function has variously been linked to (a) altering chromatin
612 confirmation, often through interaction with histone modifying proteins or histone proteins
613 themselves, (b) direct interference with transcription factor binding or function and (c) physical
614 spreading of long-range oligomeric corepressor complexes across regions of regulatory DNA
615 (Perissi et al., 2010). Dissection of the importance of each modality in Tup1 repression has
616 been challenging (Lee et al., 2000; Zhang and Reese, 2004). The tour-de-force of corepressor
617 mechanism studies in yeast concluded that the primary function of Tup1 was to physically block
618 activators (Wong and Struhl, 2011). In their work, the authors utilized the Anchor Away
619 approach to correlate the importance of HDACs, transcriptional machinery and chromatin
620 remodeling enzymes to the repression state of endogenously repressed Cyc8-Tup1 target
621 genes. They observed that Tup1 did not block the binding of transcription factors but inhibited
622 the recruitment of one Mediator component in the tail domain, GAL11/MED15, as well as Pol-II
623 and the chromatin remodelers Snf2 and Sth1. They additionally observed that HDACs had only
624 a supportive role in reinforcing Tup1 repression. These results led to their hypothesis that Tup1
625 blocks the activation domains of transcription factors, and suggested this was through direct
626 binding to activation domains (Wong and Struhl, 2011).
627 The synthetic system used here allowed us to build on this model and further refine our
628 understanding of TPL's repressive activity. In our experiments we see a similar set of
629 conditions, with TPL recruited to the DNA-bound transcriptional activator (ARF), and several
630 possible mechanisms of repression. Unlike Tup1, we have subdivided the TPL protein to identify
631 interactions between TPL and individual protein interactors with no effect on yeast function. In
632 these experiments we can eliminate the possibility that TPL blocks ARF activation by directly
633 blocking the transcription factor activation domains because we see a loss of repression only
634 when TPL-MED21 binding is eliminated through specific point mutations (Figure 4H). Our
635 inducible swap of MED21 isoforms also corroborates these findings (Figure 4), as the SLARC
636 remains genetically identical in these strains, indicating that TPL-MED21 interaction is
637 regulating activity not a TPL-ARF interaction. Furthermore, our results correlate well with
638 findings that repressed targets are reactivated when this portion of MED21 is deleted in yeast
639 (TPL - Figure 4, Tup1 - (Gromöller and Lehming, 2000)). Therefore, we suggest that instead of
640 directly binding activation domains that TPL (and likely Tup1) binds to components of Mediator

641 (MED21, MED10B and possibly others) recruited by the transcription factor. Indeed, it is easier
642 to rationalize that the repressor binds the same domains of the Mediator complex recruited by
643 the transcription factor's activation domain (with the same affinity) as opposed to binding each
644 diverse activation domain (with varying affinity). In this model, corepressor binding blocks
645 formation of a fully active Mediator complex thereby limiting Polymerase II recruitment and
646 promoter escape (Petrenko et al., 2017).

647 Multiple points of contact likely exist between the Mediator complex and other parts of
648 the transcriptional machinery in both transcriptionally repressed and active states. For auxin
649 response, specifically, there are several lines of evidence to support this model, including
650 documented association between the structural backbone of Mediator, MED14, and activated
651 and repressed auxin loci in *Arabidopsis* (Ito et al., 2016). In addition, MED12 and MED13 are
652 required for auxin-responsive gene expression in the root, and MED12 acts upstream of AUX1
653 in the root growth response to sugar (Raya-González et al., 2018). MED18 in the head module
654 represses auxin signaling and positively regulates the viability of the root meristem (Raya-
655 González et al., 2018). PFT1/MED25 regulates auxin transport and response in the root (Raya-
656 González et al., 2014). MED7, MED21's partner protein in the hinge domain, is required for
657 normal root development and loss of MED7 function impacts expression of auxin signaling
658 components (Kumar et al., 2018). Previous research identified the Mediator CDK8 subunit,
659 specifically MED13 (MAB2), as an interactor with the full-length TPL protein (Ito et al., 2016).
660 We could not observe interaction between the N-terminal domain of TPL and AtMED13,
661 AtCYC8, or AtCYCC (Supplemental Figure 1B), suggesting that any direct interactions occur
662 outside the N188 fragment. As suggested by Ito and colleagues (Ito et al., 2016) and supported
663 by our synthetic system, auxin-induced removal of TPL is sufficient to induce changes in the
664 composition of the Mediator complex, facilitating both rapid activation and rapid return to a
665 repressed basal state.

666 The conserved interaction of both TPL and Tup1 with Mediator has implications for
667 modeling the dynamics of eukaryotic transcription (e.g., (Estrada et al., 2016)). By stabilizing the
668 Mediator complex, TPL (and by extension Tup1) may create a 'pre-paused' state that allows
669 rapid recruitment of Pol-II and activation once TPL is removed. Alternatively, TPL could allow for
670 recruitment of a poised or paused Pol-II, allowing for rapid activation (and re-activation) of a
671 repressed locus. Support for this idea comes from the genome-wide correlation between
672 Groucho corepressor binding and polymerase pausing in *Drosophila* (Kaul et al., 2014).

673 However, in non-metazoan lineages (i.e. plants and yeast) the existence of bona fide pausing is
674 disputed, mainly due to the absence of the pausing regulator Negative Elongation Factor
675 complex (NELF, (Gaertner and Zeitlinger, 2014)). One possibility is that plants and yeast have
676 an ancestral or alternative form of pausing that is NELF-independent. Support for this idea
677 comes from studies of *Arabidopsis* where Pol-II was found to be markedly enriched at the five-
678 prime ends of genes, the same pattern seen with metazoan pausing (Zhu et al., 2018). In yeast,
679 Tup1 has been implicated in a form of transcriptional memory that involves recruiting a poised
680 form of preinitiation Pol-II to allow rapid reactivation of genes involved in sugar utilization (Sood
681 et al., 2017).
682
683
684 **Methods**
685
686 **Cloning**
687 Construction of TPL-IAA3 and TPL-IAA14 fusion proteins were performed as described in
688 (Pierre-Jerome et al., 2014). Variant and deletion constructs were created using PCR-mediated
689 site-directed mutagenesis. Site-directed mutagenesis primers were designed using
690 NEBasechanger and implemented through Q5® Site-Directed Mutagenesis (NEB, Cat
691 #E0554S). TPL interactor genes were amplified as cDNAs from wild type Col-0 RNA using
692 reverse transcriptase (SuperScript™ IV Reverse Transcriptase, Invitrogen) and gene-specific
693 primers from IDT (Coralville, Iowa), followed by amplification with Q5 polymerase (NEB). These
694 cDNAs were subsequently cloned into Plasmids for cytoSUS using a Gibson approach (Gibson
695 et al., 2009), through the Aquarium Biofabrication facility (Ben Keller et al., 2019). The coding
696 sequence of the genes of interest were confirmed by sequencing (Genewiz; South Plainfield,
697 NJ). For UAS driven constructs, the TPLN188-IAA14 coding sequence was amplified with
698 primers containing engineered BsaI sites and introduced into the pGII backbone with the UAS
699 promoter and RBSC terminator (Siligato et al., 2016) using Golden Gate cloning (Weber et al.,
700 2011). Subsequent mutations were performed on this backbone using PCR-mediated site-
701 directed mutagenesis (see above). Construction of C-terminal 2xFRB fusions for Anchor Away
702 were constructed as described in (Haruki et al., 2008). Inducible MED21 was constructed as
703 described in (McIsaac et al., 2013). For cell type specific knockdown mediated by dCas9-
704 TPLN300, Gibson cloning was used modify the pHEE401E plasmid, replacing the egg-specific

705 promoter and Cas9 from pHEE401E (Wang et al., 2015) with UAS promoter and dCas9-
706 TPLN300 fusion protein (Khakhar et al., 2018). The resulting plasmid is used as starting point to
707 clone 3 sgRNAs targeting the *AtMED21* promoter (identified using CHOP CHOP (Labun et al.,
708 2019). sgRNAs: GACGCAGAGTCTGTTGGGTGTGG, TTTAAAATGGGCTTTTAAGGTGG,
709 AACACTGAAGTAGAATTGGGTGG ranging from -170 to +90 region from the TSS) using PCR
710 and Golden Gate cloning strategy described in (Wang et al., 2015).
711
712 **Flow Cytometry**
713 Fluorescence measurements were taken using a Becton Dickinson (BD) special order
714 cytometer with a 514-nm laser exciting fluorescence that is cut off at 525 nm prior to
715 photomultiplier tube collection (BD, Franklin Lakes, NJ). Events were annotated, subset to
716 singlet yeast using the FlowTime R package (Wright et al., 2019). A total of 10,000 - 20,000
717 events above a 400,000 FSC-H threshold (to exclude debris) were collected for each sample
718 and data exported as FCS 3.0 files for processing using the flowCore R software package and
719 custom R scripts (Supplemental File 1, (Havens et al., 2012; Pierre-Jerome et al., 2017)). Data
720 from at least two independent replicates were combined and plotted in R (ggplots2).
721
722 **Yeast Methods**
723 Standard yeast drop-out and yeast extract–peptone–dextrose plus adenine (YPAD) media were
724 used, with care taken to use the same batch of synthetic complete (SC) media for related
725 experiments. A standard lithium acetate protocol (Gietz and Woods, 2002) was used for
726 transformations of digested plasmids. All cultures were grown at 30°C with shaking at 220 rpm.
727 Anchor-Away approaches were followed as described in (Haruki et al., 2008), and anchor away
728 strains were obtained from EURO-SCARF (euroscarf.de). Endogenous genomic fusions of
729 ScMed21-FRB were designed by fusing MED21 homology to the pFA6a-FRB-KanMX6 plasmid
730 for chromosomal integration into the parental anchor away strain as in (Petrenko et al., 2017),
731 selectable through G418 resistance (G418, Geneticin, Thermo Fisher Scientific). Tup1-FRB and
732 Cyc8-FRB were constructed as described in (Wong and Struhl, 2011). Mediator anchor away
733 strains were created in (Petrenko et al., 2017) and kindly donated by Dr. Kevin Struhl. SLARC
734 construction required a redesign of promoters and terminators used in the *At*ARC$^{Sc}$ to eliminate
735 any repetitive DNA sequences (See Figure 4 – Figure Supplement 1), using a Golden Gate
736 cloning approach into level 1 vectors. Subsequent assembly of individual transcriptional units

737 into a larger plasmid utilized VEGAS assembly which was performed as described in (Mitchell et
738 al., 2015). To create an acceptor plasmid for the assembled transcriptional units, we
739 synthesized a custom vector containing VA1 and VA2 homology sites for recombination (Twist
740 Bioscience, South San Francisco, CA). In between these sites we incorporated a pLac:mRFP
741 cassette to allow identification of uncut destination plasmid in *E. coli*, flanked by EcoRI sites for
742 linearization. Finally, the CEN6/ARSH4 was transferred from pRG215 (Addgene #64525) into
743 the acceptor plasmid by Golden Gate reaction using designed BsmBI sites engineered into the
744 acceptor plasmid and the primers used to amplify the CEN/ARS (See Figure 4 – Figure
745 Supplement 1). For the cytoplasmic split-ubiquitin protein-protein interaction system, bait and
746 prey constructs were created using the plasmids pMetOYC and pNX32, respectively (Addgene,
747 https://www.addgene.org/Christopher_Grefen/). Interaction between bait and prey proteins were
748 evaluated using a modified version of the split ubiquitin technique (Asseck and Grefen, 2018).
749 After two days of growth on control and selection plates, images were taken using a flatbed
750 scanner (Epson America, Long Beach, CA). Inducible ScMed21 strains (iMed21) were grown
751 overnight, and then diluted back to 100 events per microliter as determined by flow cytometry
752 and grown at 30C with 250rpm in a deepwell 96-well plate format. Strains were supplemented
753 with β-estradiol (20μM) for 4 hours followed by Rapamycin addition. Samples were analyzed by
754 flow cytometry throughout these growth experiments.
755
756 **Western Blot**
757 Yeast cultures that had been incubated overnight in synthetic complete (SC) media were diluted
758 to OD600 = 0.6 and incubated until cultures reached OD600 ~1. Cells were harvested by
759 centrifugation. Cells were lysed by vortexing for 5 min in the presence of 200 μl of 0.5-mm
760 diameter acid washed glass beads and 200 μl SUMEB buffer (1% SDS, 8 M urea, 10 mM
761 MOPS pH 6.8, 10 mM EDTA, 0.01% bromophenol blue, 1mM PMSF) per one OD unit of original
762 culture. Lysates were then incubated at 65° for 10 min and cleared by centrifugation prior to
763 electrophoresis and blotting. Antibodies: Anti-HA-HRP (REF-12013819001, Clone 3F10,
764 Roche/Millipore Sigma, St. Louis, MO), Anti-FLAG (F3165, Monoclonal ANTI-FLAG® M2,
765 Millipore Sigma, St. Louis, MO), Anti-FRB (ALX-215-065-1, Enzo Life Sciences, Farmingdale,
766 NY, (Haruki et al., 2008)), Anti-VP16 (1-21) (sc-7545, Santa Cruz Biotechnology, Dallas TX),
767 Anti-GFP (ab290, AbCam, Cambridge, United Kingdom), Anti-MYC (71d10, 2278S, Cell
768 Signaling, Danvers, MA), Anti-PGK1 (ab113687, AbCam, Cambridge, United Kingdom).

769

770 **Protein expression and purification**

771 All multimer deficient TPL proteins were expressed in *Escherichia coli* Rosetta 2 strain. Bacteria
772 cultures were grown at 37ºC until they achieved an $OD^{600}$nm of 0.6-0.9. Protein expression was
773 induced with isopropyl-β-D-1-thyogalactopiranoside (IPTG) at a final concentration of 400 µM at
774 18 °C overnight. Bacteria cultures were centrifuged and the pellets were resuspended in the
775 buffer A (CAPS 200 mM pH 10.5, NaCl 500 mM, TCEP 1 mM), where cells were lysed by
776 sonication. His-tagged AtTPL188 (wt and mutants) bacteria pellets were resuspended in buffer
777 A with EDTA-free antiprotease (Roche). The soluble fractions recovered after sonication were
778 passed through a Ni-sepharose (GE Healthcare) column previously washed with buffer A and
779 the bound proteins were eluted with buffer A with 250 mM imidazole. A second purification step
780 was carried out on Gel filtration Superdex 200 10/300 GL (GE Healthcare) equilibrated with
781 buffer A.

782

783 **Co-Immunoprecipitation**

784 Co-IP from yeast was performed using the cytoSUS strains. Cultures were grown to OD600 0.5
785 (~1E7 cells/ml) using selective media, harvested, and resuspended in 200 µl SUME (1% SDS,
786 8M Urea, 10mM MOPS, pH 6.8, 10mM EDTA) buffer with protease inhibitors. Cells were lysed
787 by vortexing 3 X 1 min full speed with 100 µl of 0.5 mm Acid Washed Glass Beads, clarified by
788 centrifugation (1 min, 1000rpm), and supernatant was mixed with 1ml IP buffer (15mM
789 Na2HPO4, mw 142; 150mM NaCl, mw 58; 2% Triton X-100, 0.1% SDS, 0.5% DOC, 10mM
790 EDTA, 0.02% NaN3) with protease inhibitors, and incubated with 100 µl of IgG sepharose at
791 25°C for 2 hours with rotation. The Beads were washed 1x with IP buffer, and 2x with IP-Wash
792 buffer (50mM NaCl, mw58; 10mM TRIS, mw 121; 0.02% NaN3) with protease inhibitors. Protein
793 was eluted with 50 µl of SUME buffer + 0.005% bromophenol blue by incubation at 65°C for 10
794 minutes and run on handmade 12% acrylamide SDS-PAGE gels, and western blotted
795 accordingly. Co-IPs from tobacco were performed on leaves two days after injection as
796 described in (Song et al., 2014). For Co-IPs with HA, extracts were incubated with Anti-HA-
797 Biotin (High Affinity (3F10), Sigma, 12158167001) and Streptavidin conjugated magnetic beads
798 (). For Co-IPs with MED10B-MEC-ProtA we used IgG Sepharose® 6 Fast Flow (Sigma, GE17-
799 0969-01) beads and increased washing steps (1xIP buffer, 4xWash buffer, 5 total). The only
800 modification to buffers was an addition of the detergent NP-40 at 0.1% in the IP and wash

801 buffer. Samples were run on handmade 10% acrylamide SDS-PAGE gels, and western blotted
802 accordingly.
803
804 **Bimolecular Fluorescence Complementation (BiFC)**
805 Bimolecular fluorescent complementation experiments were performed on 3-week-old *N.*
806 *benthamiana* plants grown at 22°C under long days (16 h light/8 h dark) on soil (Sunshine #4
807 mix) as per (Martin et al., 2009). pSITE vectors were used to generate BiFC constructs for
808 MED21, Δ5-MED21, TPL and $TPL^{H8QuadA}$ – proteins (Martin et al., 2009). In all cases the
809 combinations are N-terminal fusions of either the nEYFP or cEYFP to the cDNA of MED21 or
810 TPL. RFP fused Histone H2B was used as a nuclear marker (Goodin et al., 2002). Injection of
811 Agrobacterium strains into tobacco leaves was performed as in (Goodin et al., 2002), but the
812 $OD_{600}$ of the Agrobacterium culture used was adjusted to 0.5. Two days after transfection, plant
813 leaves were imaged using an epifluorescence microscope (Leica Biosystems, model: DMI
814 3000B).
815
816 **Protein alignments**
817 The MED21 protein sequence was were aligned to homologs using CLC Sequence Viewer 7, a
818 tree was constructed using a Neighbor-Joining method, and bootstrap analysis performed with
819 10,000 replicates.
820
821 **Plant growth**
822 For synthetic repression assays in tobacco Agrobacterium-mediated transient transformation of
823 *Nicotiana benthamiana* was performed as per (Yang et al., 2000). 5 ml cultures of
824 Agrobacterium strains were grown overnight at 30C shaking at 220rpm, pelleted and incubated
825 in MMA media (10 mM MgCl2, 10 mM MES pH 5.6, 100 µM acetosyringone) for 3 hours at room
826 temperature with rotation. Strain density was normalized to an OD600 of 1 for each strain in the
827 final mixture of strains before injection into tobacco leaves. Leaves were removed, and 8
828 different regions were excised using a hole punch, placed into a 96-well microtiter plate with
829 100µl of water. Each leaf punch was scanned in a 4x4 grid for yellow and red fluorescence
830 using a plate scanner (Tecan Spark, Tecan Trading AG, Switzerland). Fluorescence data was
831 quantified and plotted in R (ggplots). For *Arabidopsis thaliana* experiments using the GAL4-UAS
832 system (Laplaze et al., 2005), J0121 was introgressed eight times into Col-0 accession from the

833 C24 accession, and rigorously checked to ensure root growth was comparable to Col-0 before
834 use. UAS-TPL-IAA14$^{mED}$ constructs were introduced to J0121 introgression lines by floral dip
835 method (Clough and Bent, 1998). T1 seedlings were selected on 0.5X LS (Caisson
836 Laboratories, Smithfield, UT) + 25µg/ml Hygromycin B (company) + 0.8% phytoagar
837 (Plantmedia; Dublin, OH). Plates were stratified for 2 days, exposed to light for 6 h, and then
838 grown in the dark for 3 d following a modification of the method of (Harrison et al., 2006).
839 Hygromycin resistant seedlings were identified by their long hypocotyl, enlarged green leaves
840 and long root. Transformants were transferred by hand to fresh 0.5X LS plates + 0.8% Bacto
841 agar (Thermo Fisher Scientific) and grown vertically for 14 days at 22°C. Plates were scanned
842 on a flatbed scanner (Epson America, Long Beach, CA) at day 14. *slr* and *med21/MED21*
843 (WiscDsLox461-464K13) seeds were obtained from the Arabidopsis Biological Resource Center
844 (Columbus, OH). CRISPR/CAS9 based mutations in AtMED2 were generated as described in
845 (Wang et al., 2015). We created a novel mutation in *AtMED21* that introduces a single base-pair
846 insertion of G at nucleotide 214 after the A of the start codon (i214G). This mutation alters the
847 amino acid sequence starting at residue 25 and creates an early stop codon after 11 random
848 amino acids (Supplemental Figure 6D).
849
850 **Data submissions**
851 All flow cytometry data will be deposited at https://flowrepository.org/. All plasmids will be
852 deposited through Addgene at https://www.addgene.org/Jennifer_Nemhauser/.
853
854 **Acknowledgements**
855 We would like to thank Prof. Jef Boeke for kindly providing VEGAS adaptor and regulatory
856 element plasmids; Dr. Jennifer Brophy and Prof. José Dinneny for kindly providing the
857 pUBQ10:GAL4:VP16 plasmid; Dr. Natalia Petrenko and Dr. Kevin Struhl for kindly providing
858 Mediator anchor away strains; and Prof. Grant Brown and Prof. Maitreya Dunham for advice on
859 yeast genetics and approaches. We thank members of the Nemhauser group including Amy
860 Lanctot, Romi Ramos, Eric Yang, and Dr. Sarah Guiziou for constructive discussions and
861 comments on this manuscript. We also thank Morgan Hamm for the custom R script used here
862 to analyze anchor away plates.
863
864 **Author Contributions**

Conceptualization: ARL, JLN; Investigation: ARL, WW, HPG, SG, SJS, MLZ, JEZ; Software: ARL, HPG; Formal Analysis: ARL, HPG; Visualization: ARL, WW, HPG, SG, SJS, MLZ, JEZ; Writing-Original Draft: ARL; Writing-Review & Editing: WW, HPG, SG, SJS, MLZ, JEZ, NZ, JLN; Supervision, Project administration, Funding Acquisition, Resources: JLN, NZ.

**Declaration of Interests**

The authors declare no competing interests.

**Funding**

National Institutes of Health (NIH): ARL, HPG, SG, SJS, JEZ, MZ & JLN R01- GM107084.

Howard Hughes Medical Institute (HHMI): ARL, SJS, JEZ, MZ & JLN - Faculty Scholar Award.

Ning Zheng is a Howard Hughes Medical Institute Investigator.

ARL is supported by the Simons Foundation through the Life Science Research Foundation.

879 **References**


880 Adams, G.E., Chandru, A., and Cowley, S.M. (2018). Co-repressor, co-activator and general
881 transcription factor: the many faces of the Sin3 histone deacetylase (HDAC) complex. Biochem.
882 J. *475*, 3921–3932.

883 Agarwal, M., Kumar, P., and Mathew, S.J. (2015). The Groucho/Transducin-like enhancer of
884 split protein family in animal development. IUBMB Life *67*, 472–481.

885 Asseck, L.Y., and Grefen, C. (2018). Detecting Interactions of Membrane Proteins: The Split-
886 Ubiquitin System. Methods Mol. Biol. Clifton NJ *1794*, 49–60.

887 Baumli, S., Hoeppner, S., and Cramer, P. (2005). A Conserved Mediator Hinge Revealed in the
888 Structure of the MED7·MED21 (Med7·Srb7) Heterodimer. J. Biol. Chem. *280*, 18171–18178.

889 Ben Keller, Justin Vrana, Abraham Miller, Garrett Newman, and Eric Klavins (2019). Aquarium:
890 The Laboratory Operating System (Zenodo).

891 Biddick, R., and Young, E.T. (2005). Yeast Mediator and its role in transcriptional regulation. C.
892 R. Biol. *328*, 773–782.

893 Bourbon, H.-M. (2008). Comparative genomics supports a deep evolutionary origin for the large,
894 four-module transcriptional mediator complex. Nucleic Acids Res. *36*, 3993–4008.

895 Brand, A.H., and Perrimon, N. (1993). Targeted gene expression as a means of altering cell
896 fates and generating dominant phenotypes. Dev. Camb. Engl. *118*, 401–415.

897 Busch, W., Miotk, A., Ariel, F.D., Zhao, Z., Forner, J., Daum, G., Suzaki, T., Schuster, C.,
898 Schultheiss, S.J., Leibfried, A., et al. (2010). Transcriptional control of a plant stem cell niche.
899 Dev. Cell *18*, 849–861.

900 Causier, B., Ashworth, M., Guo, W., and Davies, B. (2012). The TOPLESS interactome: a
901 framework for gene repression in Arabidopsis. Plant Physiol. *158*, 423–438.

902 Chen, G., and Courey, A.J. (2000). Groucho/TLE family proteins and transcriptional repression.
903 Gene *249*, 1–16.

904 Clough, S.J., and Bent, A.F. (1998). Floral dip: a simplified method for Agrobacterium-mediated
905 transformation of Arabidopsis thaliana. Plant J. Cell Mol. Biol. *16*, 735–743.

906 Collins, J., O'Grady, K., Chen, S., and Gurley, W. (2019). The C-terminal WD40 repeats on the
907 TOPLESS co-repressor function as a protein–protein interaction surface. Plant Mol. Biol. *100*,
908 47–58.

909 Delto, C.F., Heisler, F.F., Kuper, J., Sander, B., Kneussel, M., and Schindelin, H. (2015). The
910 LisH motif of muskelin is crucial for oligomerization and governs intracellular localization. Struct.
911 Lond. Engl. 1993 *23*, 364–373.

912 Dhawan, R., Luo, H., Foerster, A.M., Abuqamar, S., Du, H.-N., Briggs, S.D., Mittelsten Scheid,
913 O., and Mengiste, T. (2009). HISTONE MONOUBIQUITINATION1 interacts with a subunit of the
914 mediator complex and regulates defense against necrotrophic fungal pathogens in Arabidopsis.
915 Plant Cell *21*, 1000–1019.

916 Dolan, W.L., and Chapple, C. (2017). Conservation and Divergence of Mediator Structure and
917 Function: Insights from Plants. Plant Cell Physiol. *58*, 4–21.

918 Estrada, J., Wong, F., DePace, A., and Gunawardena, J. (2016). Information Integration and
919 Energy Expenditure in Gene Regulation. Cell *166*, 234–244.

920 Flanagan, P.M., Kelleher, R.J., Sayre, M.H., Tschochner, H., and Kornberg, R.D. (1991). A
921 mediator required for activation of RNA polymerase II transcription in vitro. Nature *350*, 436–
922 438.

923 Flowers, E.B., Poole, R.J., Tursun, B., Bashllari, E., Pe'er, I., and Hobert, O. (2010). The
924 Groucho ortholog UNC-37 interacts with the short Groucho-like protein LSY-22 to control
925 developmental decisions in C. elegans. Dev. Camb. Engl. *137*, 1799–1805.

926 Fukaki, H., Tameda, S., Masuda, H., and Tasaka, M. (2002). Lateral root formation is blocked
927 by a gain-of-function mutation in the SOLITARY-ROOT/IAA14 gene of Arabidopsis. Plant J. Cell
928 Mol. Biol. *29*, 153–168.

929 Gaertner, B., and Zeitlinger, J. (2014). RNA polymerase II pausing during development.
930 Development *141*, 1179–1183.

931 Gasperowicz, M., and Otto, F. (2005). Mammalian Groucho homologs: redundancy or
932 specificity? J. Cell. Biochem. *95*, 670–687.

933 Gibson, D.G., Young, L., Chuang, R.-Y., Venter, J.C., Hutchison, C.A., and Smith, H.O. (2009).
934 Enzymatic assembly of DNA molecules up to several hundred kilobases. Nat. Methods *6*, 343–
935 345.

936 Gietz, R.D., and Woods, R.A. (2002). Transformation of yeast by lithium acetate/single-stranded
937 carrier DNA/polyethylene glycol method. Methods Enzymol. *350*, 87–96.

938 Gonzalez, N., Pauwels, L., Baekelandt, A., De Milde, L., Van Leene, J., Besbrugge, N.,
939 Heyndrickx, K.S., Cuéllar Pérez, A., Durand, A.N., De Clercq, R., et al. (2015). A Repressor
940 Protein Complex Regulates Leaf Growth in Arabidopsis. Plant Cell *27*, 2273–2287.

941 Goodin, M.M., Dietzgen, R.G., Schichnes, D., Ruzin, S., and Jackson, A.O. (2002). pGD
942 vectors: versatile tools for the expression of green and red fluorescent protein fusions in
943 agroinfiltrated plant leaves. Plant J. Cell Mol. Biol. *31*, 375–383.

944 Grbavec, D., Lo, R., Liu, Y., and Stifani, S. (1998). Transducin-like Enhancer of split 2, a
945 mammalian homologue of Drosophila Groucho, acts as a transcriptional repressor, interacts
946 with Hairy/Enhancer of split proteins, and is expressed during neuronal development. Eur. J.
947 Biochem. *258*, 339–349.

948 Gromöller, A., and Lehming, N. (2000). Srb7p is a physical and physiological target of Tup1p.
949 EMBO J. *19*, 6845–6852.

950 Hallberg, M., Hu, G.-Z., Tronnersjö, S., Shaikhibrahim, Z., Balciunas, D., Björklund, S., and
951 Ronne, H. (2006). Functional and physical interactions within the middle domain of the yeast
952 mediator. Mol. Genet. Genomics MGG *276*, 197–210.

953 Haruki, H., Nishikawa, J., and Laemmli, U.K. (2008). The anchor-away technique: rapid,
954 conditional establishment of yeast mutant phenotypes. Mol. Cell *31*, 925–932.

955 Havens, K.A., Guseman, J.M., Jang, S.S., Pierre-Jerome, E., Bolten, N., Klavins, E., and
956 Nemhauser, J.L. (2012). A synthetic approach reveals extensive tunability of auxin signaling.
957 Plant Physiol. *160*, 135–142.

958 Ito, J., Fukaki, H., Onoda, M., Li, L., Li, C., Tasaka, M., and Furutani, M. (2016). Auxin-
959 dependent compositional change in Mediator in ARF7- and ARF19-mediated transcription. Proc.
960 Natl. Acad. Sci. U. S. A. *113*, 6562–6567.

961 Kagale, S., Links, M.G., and Rozwadowski, K. (2010). Genome-wide analysis of ethylene-
962 responsive element binding factor-associated amphiphilic repression motif-containing
963 transcriptional regulators in Arabidopsis. Plant Physiol. *152*, 1109–1134.

964 Kaul, A., Schuster, E., and Jennings, B.H. (2014). The Groucho co-repressor is primarily
965 recruited to local target sites in active chromatin to attenuate transcription. PLoS Genet. *10*,
966 e1004595.

967 Ke, J., Ma, H., Gu, X., Thelen, A., Brunzelle, J.S., Li, J., Xu, H.E., and Melcher, K. (2015).
968 Structural basis for recognition of diverse transcriptional repressors by the TOPLESS family of
969 corepressors. Sci. Adv. *1*, e1500107.

970 Khakhar, A., Leydon, A.R., Lemmex, A.C., Klavins, E., and Nemhauser, J.L. (2018). Synthetic
971 hormone-responsive transcription factors can monitor and re-program plant development. ELife
972 *7*.

973 Kim, M.H., Cooper, D.R., Oleksy, A., Devedjiev, Y., Derewenda, U., Reiner, O., Otlewski, J.,
974 and Derewenda, Z.S. (2004). The Structure of the N-Terminal Domain of the Product of the
975 Lissencephaly Gene Lis1 and Its Functional Implications. Structure *12*, 987–998.

976 Kim, Y.J., Björklund, S., Li, Y., Sayre, M.H., and Kornberg, R.D. (1994). A multiprotein mediator
977 of transcriptional activation and its interaction with the C-terminal repeat domain of RNA
978 polymerase II. Cell *77*, 599–608.

979 Klepikova, A.V., Kasianov, A.S., Gerasimov, E.S., Logacheva, M.D., and Penin, A.A. (2016). A
980 high resolution map of the Arabidopsis thaliana developmental transcriptome based on RNA-
981 seq profiling. Plant J. *88*, 1058–1070.

982 Krogan, N.T., Hogan, K., and Long, J.A. (2012). APETALA2 negatively regulates multiple floral
983 organ identity genes in Arabidopsis by recruiting the co-repressor TOPLESS and the histone
984 deacetylase HDA19. Dev. Camb. Engl. *139*, 4180–4190.

985 Kumar, K.R.R., Blomberg, J., and Björklund, S. (2018). The MED7 subunit paralogs of Mediator
986 function redundantly in development of etiolated seedlings in Arabidopsis. Plant J. *96*, 578–594.

987 Labun, K., Montague, T.G., Krause, M., Torres Cleuren, Y.N., Tjeldnes, H., and Valen, E.
988 (2019). CHOPCHOP v3: expanding the CRISPR web toolbox beyond genome editing. Nucleic
989 Acids Res. *47*, W171–W174.

990 Laplaze, L., Parizot, B., Baker, A., Ricaud, L., Martinière, A., Auguy, F., Franche, C., Nussaume,
991 L., Bogusz, D., and Haseloff, J. (2005). GAL4-GFP enhancer trap lines for genetic manipulation
992 of lateral root development in Arabidopsis thaliana. J. Exp. Bot. *56*, 2433–2442.

993 Lee, J.E., and Golz, J.F. (2012). Diverse roles of Groucho/Tup1 co-repressors in plant growth
994 and development. Plant Signal. Behav. *7*, 86–92.

995 Lee, M., Chatterjee, S., and Struhl, K. (2000). Genetic analysis of the role of Pol II holoenzyme
996 components in repression by the Cyc8-Tup1 corepressor in yeast. Genetics *155*, 1535–1542.

997 Liu, Z., and Karmarkar, V. (2008). Groucho/Tup1 family co-repressors in plant development.
998 Trends Plant Sci. *13*, 137–144.

999 Liu, X., Galli, M., Camehl, I., and Gallavotti, A. (2019). RAMOSA1 ENHANCER LOCUS2-
1000 Mediated Transcriptional Repression Regulates Vegetative and Reproductive Architecture.
1001 Plant Physiol. *179*, 348–363.

1002 Long, J.A., Ohno, C., Smith, Z.R., and Meyerowitz, E.M. (2006). TOPLESS regulates apical
1003 embryonic fate in Arabidopsis. Science *312*, 1520–1523.

1004 Ma, H., Duan, J., Ke, J., He, Y., Gu, X., Xu, T.-H., Yu, H., Wang, Y., Brunzelle, J.S., Jiang, Y., et
1005 al. (2017). A D53 repression motif induces oligomerization of TOPLESS corepressors and
1006 promotes assembly of a corepressor-nucleosome complex. Sci. Adv. *3*, e1601217.

1007 Maji, S., Dahiya, P., Waseem, M., Dwivedi, N., Bhat, D.S., Dar, T.H., and Thakur, J.K. (2019).
1008 Interaction map of Arabidopsis Mediator complex expounding its topology. Nucleic Acids Res.
1009 *47*, 3904–3920.

1010 Malik, N., Agarwal, P., and Tyagi, A. (2017). Emerging functions of multi-protein complex
1011 Mediator with special emphasis on plants. Crit. Rev. Biochem. Mol. Biol. *52*, 475–502.

1012 Martin, K., Kopperud, K., Chakrabarty, R., Banerjee, R., Brooks, R., and Goodin, M.M. (2009).
1013 Transient expression in Nicotiana benthamiana fluorescent marker lines provides enhanced
1014 definition of protein localization, movement and interactions in planta. Plant J. Cell Mol. Biol. *59*,
1015 150–162.

1016 Martin-Arevalillo, R., Nanao, M.H., Larrieu, A., Vinos-Poyo, T., Mast, D., Galvan-Ampudia, C.,
1017 Brunoud, G., Vernoux, T., Dumas, R., and Parcy, F. (2017). Structure of the Arabidopsis
1018 TOPLESS corepressor provides insight into the evolution of transcriptional repression. Proc.
1019 Natl. Acad. Sci. U. S. A.

1020 Matsumura, H., Kusaka, N., Nakamura, T., Tanaka, N., Sagegami, K., Uegaki, K., Inoue, T., and
1021 Mukai, Y. (2012). Crystal structure of the N-terminal domain of the yeast general corepressor
1022 Tup1p and its functional implications. J. Biol. Chem. *287*, 26528–26538.

1023 McIsaac, R.S., Oakes, B.L., Wang, X., Dummit, K.A., Botstein, D., and Noyes, M.B. (2013).
1024 Synthetic gene expression perturbation systems with rapid, tunable, single-gene specificity in
1025 yeast. Nucleic Acids Res. *41*, e57.

1026 Mitchell, L.A., Chuang, J., Agmon, N., Khunsriraksakul, C., Phillips, N.A., Cai, Y., Truong, D.M.,
1027 Veerakumar, A., Wang, Y., Mayorga, M., et al. (2015). Versatile genetic assembly system
1028 (VEGAS) to assemble pathways for expression in S. cerevisiae. Nucleic Acids Res. *43*, 6620–
1029 6630.

1030 Mottis, A., Mouchiroud, L., and Auwerx, J. (2013). Emerging roles of the corepressors NCoR1
1031 and SMRT in homeostasis. Genes Dev. *27*, 819–835.

1032 Oberoi, J., Fairall, L., Watson, P.J., Yang, J.-C., Czimmerer, Z., Kampmann, T., Goult, B.T.,
1033 Greenwood, J.A., Gooch, J.T., Kallenberger, B.C., et al. (2011). Structural basis for the
1034 assembly of the SMRT/NCoR core transcriptional repression machinery. Nat. Struct. Mol. Biol.
1035 *18*, 177–184.

1036 Papamichos-Chronakis, M., Conlan, R.S., Gounalaki, N., Copf, T., and Tzamarias, D. (2000).
1037 Hrs1/Med3 is a Cyc8-Tup1 corepressor target in the RNA polymerase II holoenzyme. J. Biol.
1038 Chem. *275*, 8397–8403.

1039 Perissi, V., Jepsen, K., Glass, C.K., and Rosenfeld, M.G. (2010). Deconstructing repression:
1040 evolving models of co-repressor action. Nat. Rev. Genet. *11*, 109–123.

1041 Petrenko, N., Jin, Y., Wong, K.H., and Struhl, K. (2017). Evidence that Mediator is essential for
1042 Pol II transcription, but is not a required component of the preinitiation complex in vivo. ELife *6*,
1043 e28447.

1044 Pierre-Jerome, E., Jang, S.S., Havens, K.A., Nemhauser, J.L., and Klavins, E. (2014).
1045 Recapitulation of the forward nuclear auxin response pathway in yeast. Proc. Natl. Acad. Sci. U.
1046 S. A. *111*, 9407–9412.

1047 Pierre-Jerome, E., Wright, R.C., and Nemhauser, J.L. (2017). Characterizing Auxin Response
1048 Circuits in Saccharomyces cerevisiae by Flow Cytometry. Methods Mol. Biol. Clifton NJ *1497*,
1049 271–281.

1050 Raya-González, J., Ortiz-Castro, R., Ruíz-Herrera, L.F., Kazan, K., and López-Bucio, J. (2014).
1051 PHYTOCHROME AND FLOWERING TIME1/MEDIATOR25 Regulates Lateral Root Formation
1052 via Auxin Signaling in Arabidopsis. Plant Physiol. *165*, 880–894.

1053 Raya-González, J., Oropeza-Aburto, A., López-Bucio, J.S., Guevara-García, Á.A., de Veylder,
1054 L., López-Bucio, J., and Herrera-Estrella, L. (2018). MEDIATOR18 influences Arabidopsis root
1055 architecture, represses auxin signaling and is a critical factor for cell viability in root meristems.
1056 Plant J. Cell Mol. Biol. *96*, 895–909.

1057 Samanta, S., and Thakur, J.K. (2015). Importance of Mediator complex in the regulation and
1058 integration of diverse signaling pathways in plants. Front. Plant Sci. *6*, 757.

1059 Sato, S., Tomomori-Sato, C., Tsai, K.-L., Yu, X., Sardiu, M., Saraf, A., Washburn, M.P., Florens,
1060 L., Asturias, F.J., Conaway, R.C., et al. (2016). Role for the MED21-MED7 Hinge in Assembly of
1061 the Mediator-RNA Polymerase II Holoenzyme. J. Biol. Chem. *291*, 26886–26898.

1062 Schreiber-Agus, N., Chin, L., Chen, K., Torres, R., Rao, G., Guida, P., Skoultchi, A.I., and
1063 DePinho, R.A. (1995). An amino-terminal domain of Mxi1 mediates anti-Myc oncogenic activity
1064 and interacts with a homolog of the yeast transcriptional repressor SIN3. Cell *80*, 777–786.

1065 Siligato, R., Wang, X., Yadav, S.R., Lehesranta, S., Ma, G., Ursache, R., Sevilem, I., Zhang, J.,
1066 Gorte, M., Prasad, K., et al. (2016). MultiSite Gateway-Compatible Cell Type-Specific Gene-
1067 Inducible System for Plants. Plant Physiol. *170*, 627–641.

1068 Song, Y.H., Estrada, D.A., Johnson, R.S., Kim, S.K., Lee, S.Y., MacCoss, M.J., and Imaizumi,
1069 T. (2014). Distinct roles of FKF1, GIGANTEA, and ZEITLUPE proteins in the regulation of
1070 CONSTANS stability in Arabidopsis photoperiodic flowering. Proc. Natl. Acad. Sci. *111*, 17672–
1071 17677.

1072 Sood, V., Cajigas, I., D'Urso, A., Light, W.H., and Brickner, J.H. (2017). Epigenetic
1073 Transcriptional Memory of GAL Genes Depends on Growth in Glucose and the Tup1
1074 Transcription Factor in Saccharomyces cerevisiae. Genetics *206*, 1895–1907.

1075 Ulmasov, T., Hagen, G., and Guilfoyle, T.J. (1997). ARF1, a transcription factor that binds to
1076 auxin response elements. Science *276*, 1865–1868.

1077 Wang, Z.-P., Xing, H.-L., Dong, L., Zhang, H.-Y., Han, C.-Y., Wang, X.-C., and Chen, Q.-J.
1078 (2015). Egg cell-specific promoter-controlled CRISPR/Cas9 efficiently generates homozygous
1079 mutants for multiple target genes in Arabidopsis in a single generation. Genome Biol. *16*, 144.

1080 Weber, E., Engler, C., Gruetzner, R., Werner, S., and Marillonnet, S. (2011). A Modular Cloning
1081 System for Standardized Assembly of Multigene Constructs. PLOS ONE *6*, e16765.

1082 Wong, K.H., and Struhl, K. (2011). The Cyc8-Tup1 complex inhibits transcription primarily by
1083 masking the activation domain of the recruiting protein. Genes Dev. *25*, 2525–2539.

1084 Wong, M.M., Guo, C., and Zhang, J. (2014). Nuclear receptor corepressor complexes in cancer:
1085 mechanism, function and regulation. Am. J. Clin. Exp. Urol. *2*, 169–187.

1086 Wright, R.C., Bolten, N., and Pierre-Jerome, E. (2019). flowTime: Annotation and analysis of
1087 biological dynamical systems using flow cytometry (Bioconductor version: Release (3.10)).

1088 Yang, Y., Li, R., and Qi, M. (2000). In vivo analysis of plant promoters and transcription factors
1089 by agroinfiltration of tobacco leaves. Plant J. *22*, 543–551.

1090 Zhang, Z., and Reese, J.C. (2004). Redundant Mechanisms Are Used by Ssn6-Tup1 in
1091 Repressing Chromosomal Gene Transcription in Saccharomyces cerevisiae. J. Biol. Chem.
1092 *279*, 39240–39250.

1093 Zhang, Y., Gao, S., and Wang, Z. (2010). Structural and functional analysis of amino-terminal
1094 enhancer of split in androgen-receptor-driven transcription. Biochem. J. *427*, 499–511.

1095 Zhu, J., Jeong, J.C., Zhu, Y., Sokolchik, I., Miyazaki, S., Zhu, J.-K., Hasegawa, P.M., Bohnert,
1096 H.J., Shi, H., Yun, D.-J., et al. (2008). Involvement of Arabidopsis HOS15 in histone
1097 deacetylation and cold tolerance. Proc. Natl. Acad. Sci. *105*, 4945–4950.

1098 Zhu, J., Liu, M., Liu, X., and Dong, Z. (2018). RNA polymerase II activity revealed by GRO-seq
1099 and pNET-seq in Arabidopsis. Nat. Plants *4*, 1112–1123.

1100

1101

1102
1103

1104 **Supplemental Figures**

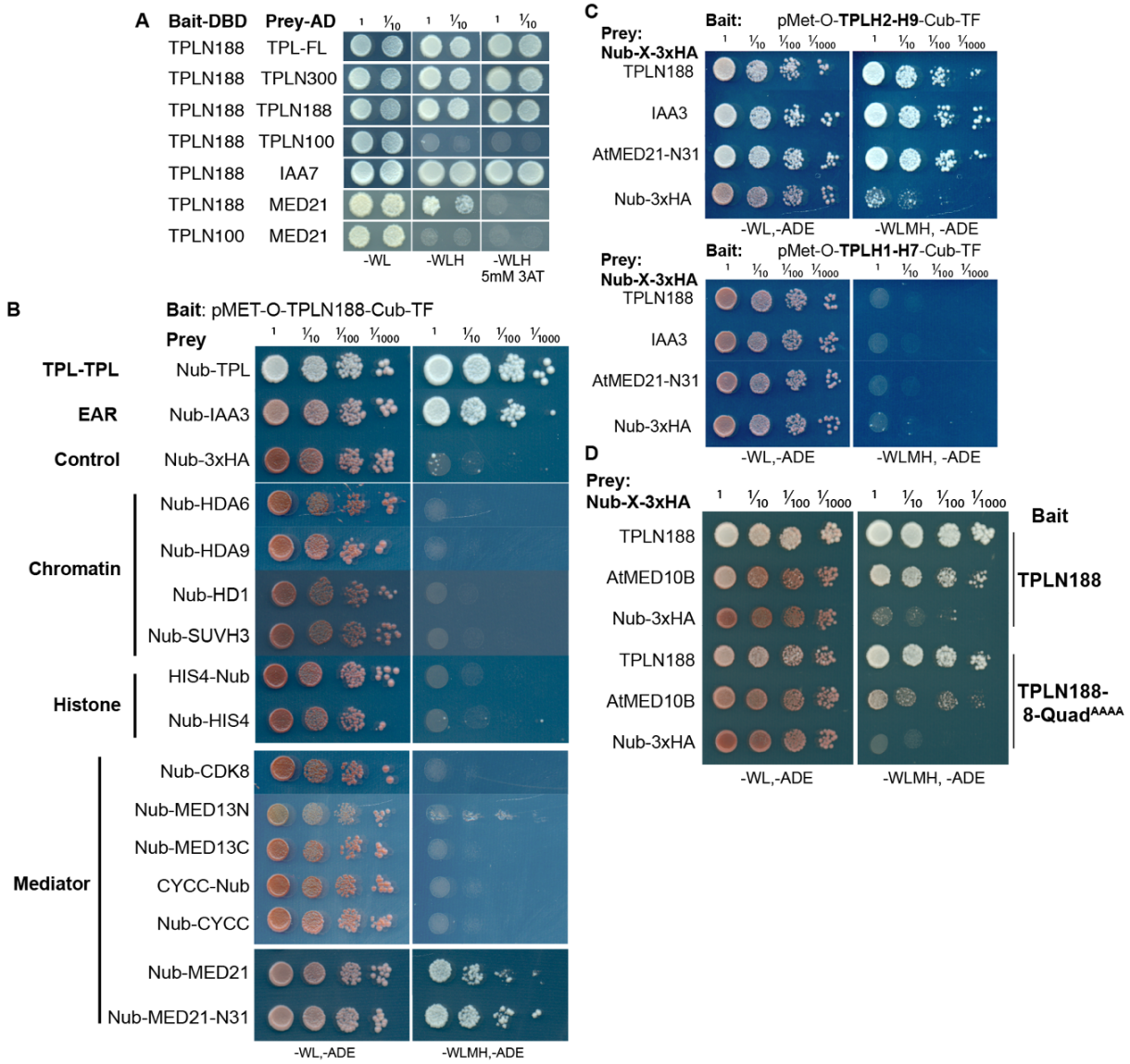


1105

1106 **Supplemental Figure 1. The TPL-N terminal domain (TPLN188) interacts with the N-**
1107 **terminus of AtMED21**. **A.** Identifying TPL-N terminal domain interactor proteins through Yeast
1108 Two Hybrid screening identifies TPL as a problematic Bait protein, as it may silence the
1109 activation despite successful binding of a prey protein (see second row from bottom where
1110 N188 and MED21 show very weak reporter activity on 3AT). 3AT - 3-Amino-1,2,4-triazole.
1111 Plates were measured after 3 days to allow TPL-MED21 interactions to grow. **B.** Identifying
1112 TPL-N terminal domain interactor proteins through cytoplasmic split ubiquitin protein interaction
1113 assay. We tested the N-terminal and C-terminal portions of MED13 separately and divided the
1114 coding sequence at amino acid 967 (MED13N = aa1-967, MED13C = aa968-1908). Each bait
1115 tested is the *Arabidopsis* homolog cloned from cDNA from the Col-0 accession, with the

1116 exception of *AtMED13*, which was synthesized *de novo* via Twist
1117 (https://www.twistbioscience.com/). Plates were scanned at 3 days after plating to allow weaker
1118 interactions to develop if they were present. **C.** TPL interacts with MED21 through an interaction
1119 within Helices 8-9. Plates were scanned at 2 days after plating. **D.** The Helix 8 Quadruple
1120 mutation (V145A, E146A, K148A, K149A) does not affect AtMED10B binding to TPL. Plates
1121 were scanned at 3 days after plating. **B-D.** The relative position of the N-terminal portion of
1122 ubiquitin (Nub) is indicated for each bait protein.

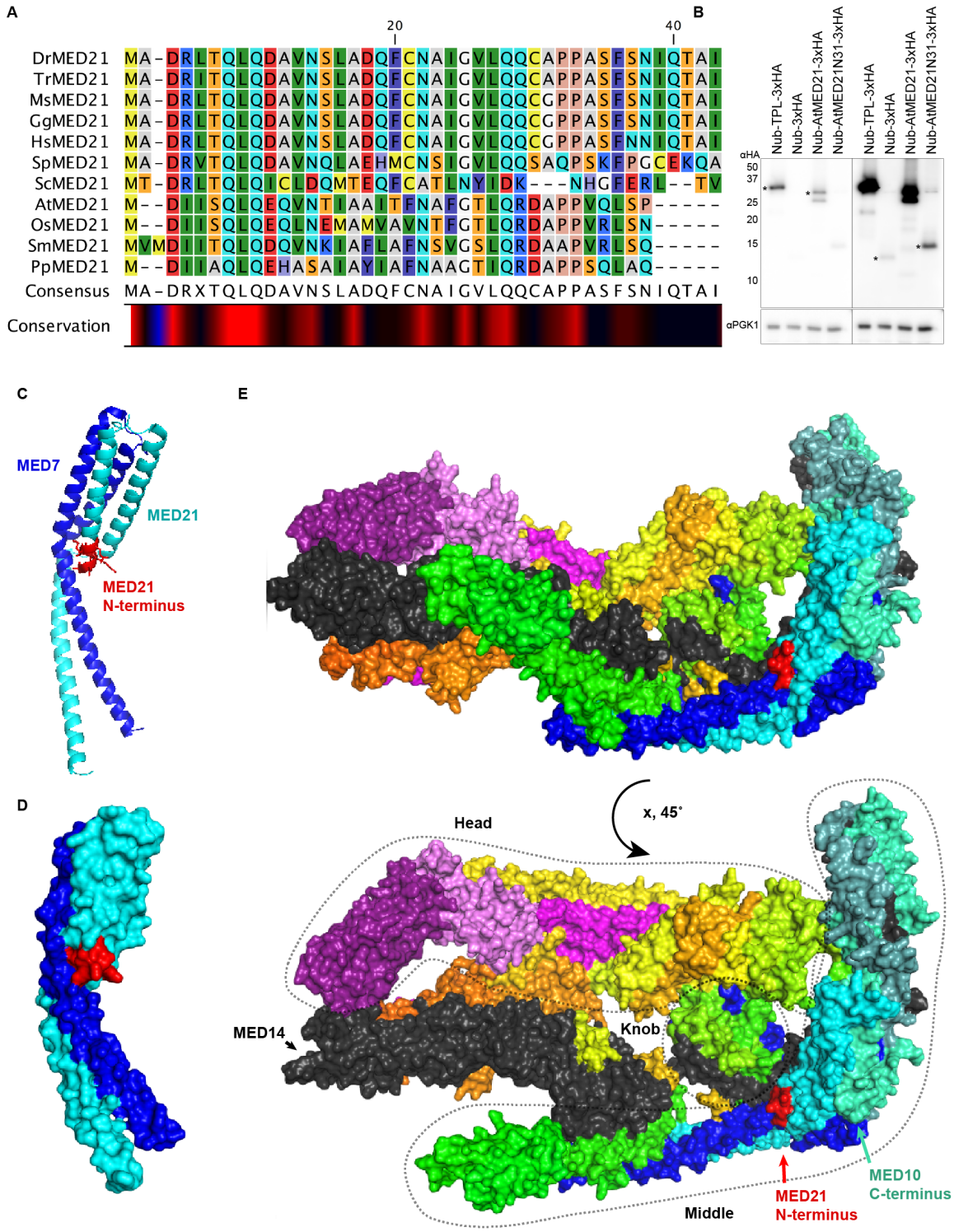


**Supplemental Figure 2. Homology and structure of the MED21 subunit of the mediator complex. A.** Protein levels of AtMED21 cytoSUS constructs in yeast. Two different exposure times are shown to demonstrate the lower abundance of the truncation with only the first 31

1127 amino acids of the AtMED21 (N31). Asterisks indicate the size predicted for the indicated
1128 protein. **B.** Protein alignment of selected MED21 homologs from various species. Dr -
1129 *Drosophila melanogaster*, Tr - *Takifugu rubripes*, Ms - *Mus musculus*, Gg - *Gallus gallus*, Hs -
1130 *Homo sapiens*, Sp - *Strongylocentrotus purpuratus*, Sc - *Saccharomyces cerevisiae*, At -
1131 *Arabidopsis thaliana*, Os - *Oryza sativa*, Sm - *Selaginella moellendorffii*, Pp - *Physcomitrella*
1132 *patens*. Alignment was performed in CLC sequence viewer 7, using a neighbor joining method.
1133 **C-D.** Structure of the MED21 (Cyan) & MED7 (Blue) hetero dimer, adapted from 1YKH, (Baumli
1134 et al., 2005). The amino acids in the N-terminus that were solved are highlighted in red up to the
1135 7th amino acid of the yeast MED21. **C.** The cartoon visualization, **D.** Surface visualization. **E.**
1136 Core mediator (5N9J, (Nozawa et al., 2017)) with the location of MED21 and MED7 indicated
1137 with the same colors from (C-D). In this structure the location of the MED21 N-terminus is again
1138 indicated in red, demonstrating its close proximity to the Knob region (dotted circle).
1139

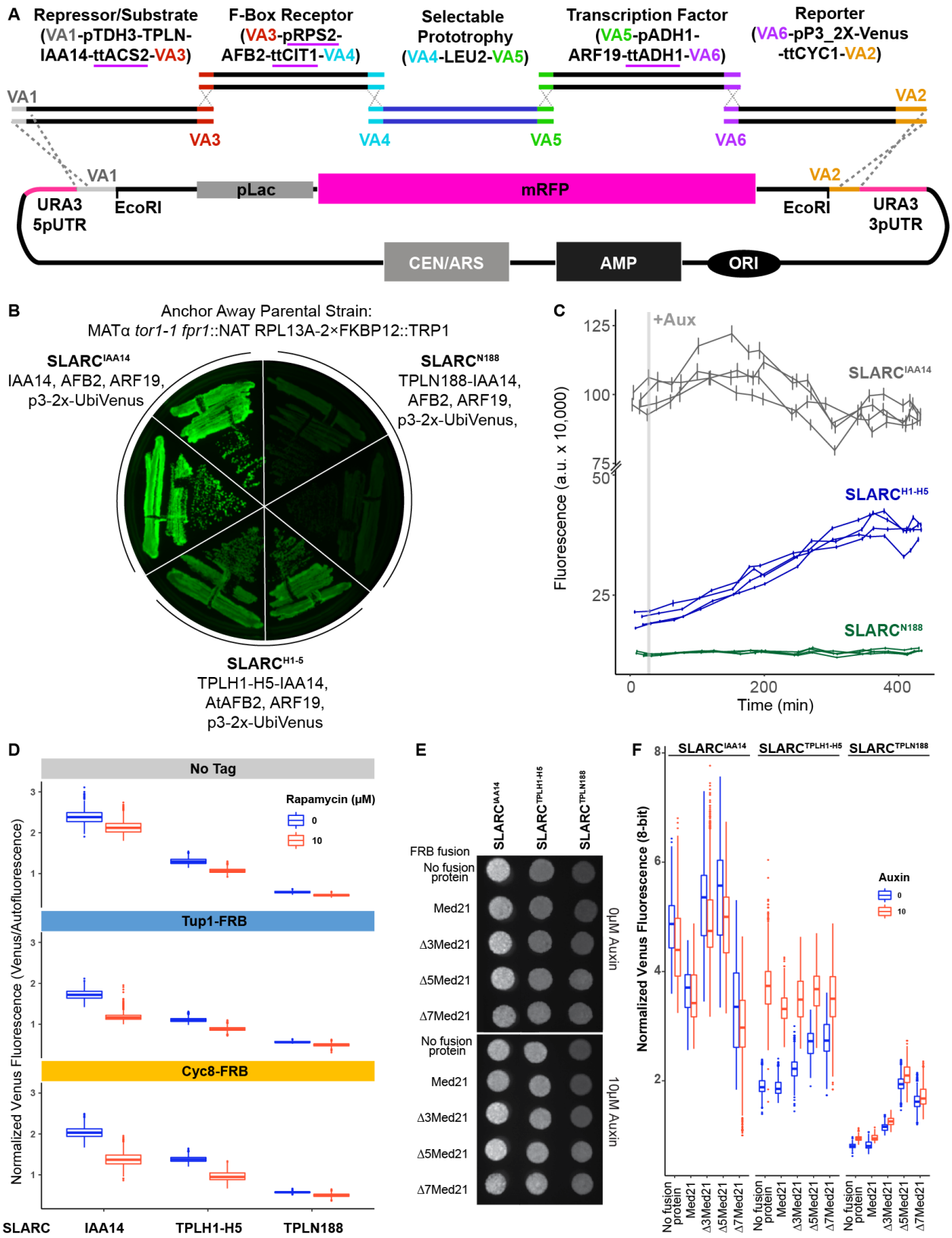
A
Repressor/Substrate (VA1-pTDH3-TPLN-IAA14-ttACS2-VA3)
F-Box Receptor (VA3-pRPS2-AFB2-ttCIT1-VA4)
Selectable Prototrophy (VA4-LEU2-VA5)
Transcription Factor (VA5-pADH1-ARF19-ttADH1-VA6)
Reporter (VA6-pP3_2X-Venus -ttCYC1-VA2)
VA1
VA2
VA3
VA4
VA5
VA6
URA3 5pUTR
EcoRI
pLac
mRFP
URA3 3pUTR
CEN/ARS
AMP
ORI
B
Anchor Away Parental Strain:
MATα tor1-1 fpr1::NAT RPL13A-2×FKBP12::TRP1
SLARCIAA14
IAA14, AFB2, ARF19, p3-2x-UbiVenus
SLARCN188
TPLN188-IAA14, AFB2, ARF19, p3-2x-UbiVenus,
SLARCH1-5
TPLH1-H5-IAA14, AtAFB2, ARF19, p3-2x-UbiVenus
C
+Aux
SLARCIAA14
SLARCH1-H5
SLARCN188
Fluorescence (a.u. x 10,000)
Time (min)
D
No Tag
Tup1-FRB
Cyc8-FRB
Rapamycin (μM)
Normalized Venus Fluorescence (Venus/Autofluorescence)
SLARC
IAA14
TPLH1-H5
TPLN188
E
SLARCIAA14
SLARCTPLH1-H5
SLARCTPLN188
FRB fusion
No fusion protein
Med21
Δ3Med21
Δ5Med21
Δ7Med21
0μM Auxin
10μM Auxin
F
SLARCIAA14
SLARCTPLH1-H5
SLARCTPLN188
Normalized Venus Fluorescence (8-bit)
Auxin

1140

1141 **Supplemental Figure 3. Construction and characterization of the Single Locus Auxin**
1142 **Response Circuit (SLARC). A.** Design schematic of the approach utilized to create the SLARC
1143 through a VEGAS assembly approach. Each individual transcriptional unit (TU) was checked to
1144 replace promoters or terminators that utilized identical sequences and replaced with an
1145 alternative sequence indicated by a purple underline. These TUs were assembled into level 1
1146 plasmids by Golden Gate reaction. Subsequently, they were amplified by PCR using primers
1147 specific for the Vegas Adaptor (VA) sequences specific for their TU cassette. In example, for the
1148 first Repressor/Substrate TU the TU was amplified using primers for VA1 and VA3 and purified
1149 by a PCR cleanup column (NEB). The acceptor plasmid was cut with EcoRI and both TU and
1150 acceptor plasmid was transformed into yeast and recombinant plasmids were selected on
1151 synthetic drop out (SDO) plates lacking Leucine. **B.** Primary SLARC transformants were struck
1152 out onto fresh SDO -Leu and imaged for Venus expression, demonstrating varying levels of
1153 reporter expression that correlate with TPL repressor domains. Plasmid DNA was purified from
1154 these strains and sequenced to confirm the proper recombination of TU cassettes. **C.** Time
1155 course flow cytometry of SLARC strains following auxin addition. For all cytometry experiments,
1156 the indicated TPL construct is fused to IAA14, because this IAA works better in haploid yeast
1157 strains that IAA3. Every point represents the average fluorescence of 5-10,000 individually
1158 measured yeast cells (a.u. - arbitrary units). Auxin (IAA-10μM) was added at the indicated time
1159 (gray bar, + Aux). Four independent experiments are shown for each construct. **D.** The yeast
1160 TPL homolog Tup1 and its partner protein Cyc8 do not repress the SLARC. Quantified
1161 fluorescence from the single locus auxin response circuit (SLARC) introduced into Tup1 and
1162 Cyc8 anchor away lines demonstrates no increased fluorescence from the reporter upon
1163 depletion of Tup1 or Cyc8 from the nucleus. Anchor away depletion of Tup1 or Cyc8 results in
1164 slower yeast growth. To normalize for this disparity in growth, Venus fluorescence was
1165 normalized to red autofluorescence, where each pixel was normalized to the corresponding red
1166 autofluorescence collected for that position and plotted as a boxplot. Two individual biological
1167 replicates (two separate experiments) were evaluated, and the data was pooled. **E-F.** Med21 N
1168 terminal deletions are viable in *Saccharomyces* and demonstrate altered SLARC transcriptional
1169 states. **E.** A representative grayscale image of fellow fluorescence of spot plates of yeast strains
1170 carrying SLARC plasmids in Med21 N-terminal deletions. Each is plated at an OD600 of 0.1 on
1171 SDO with or without auxin (10μM IAA). **F.** Venus fluorescence from (**E**) was normalized to red
1172 background (autofluorescence), where each pixel was normalized to the corresponding red

1173 autofluorescence collected for that position and plotted as a boxplot. Two individual biological
1174 replicates (two separate experiments) were evaluated, and the data was pooled and is
1175 presented as boxplots.
1176

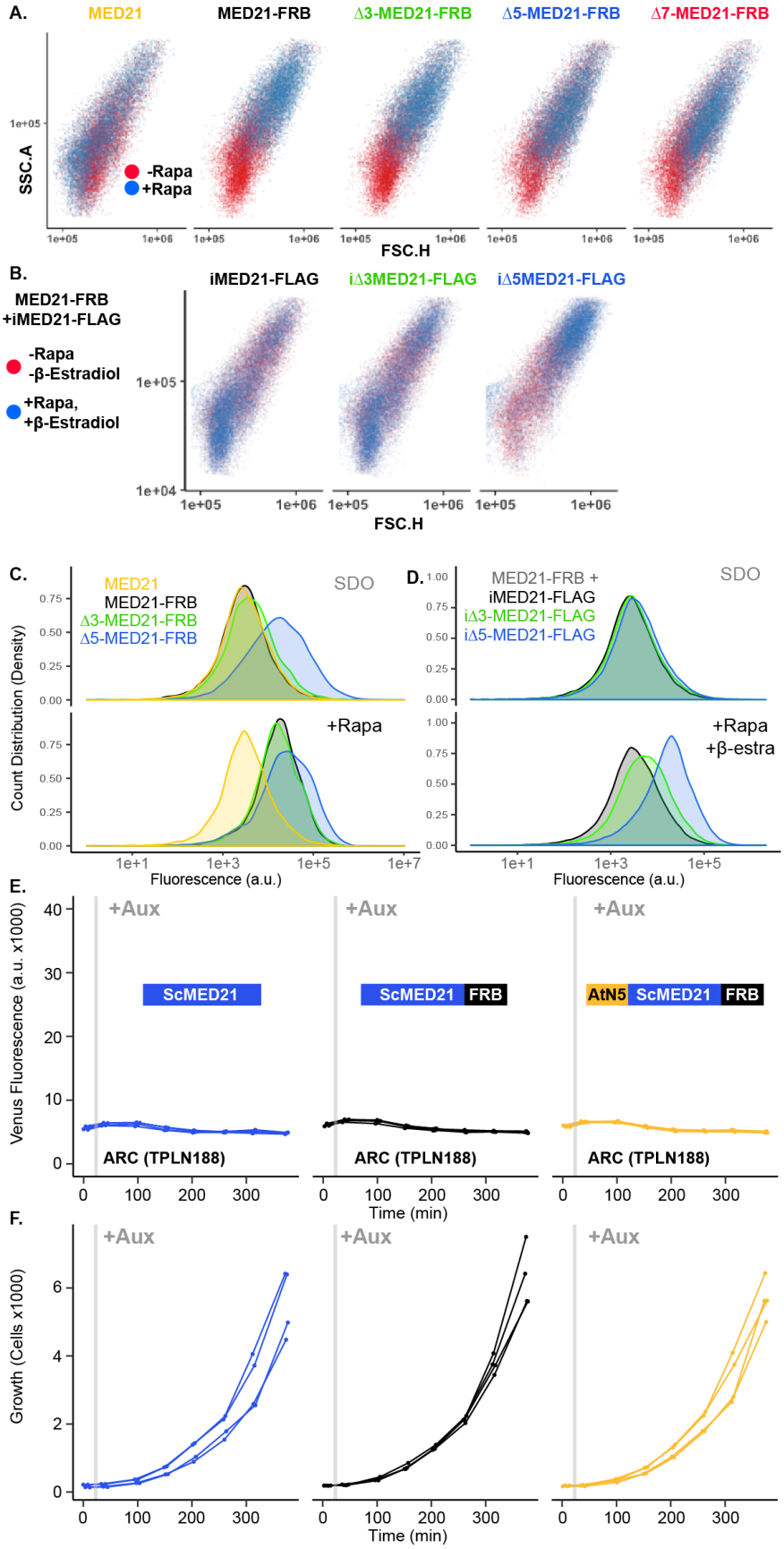
A.
MED21
MED21-FRB
Δ3-MED21-FRB
Δ5-MED21-FRB
Δ7-MED21-FRB
SSC.A
-Rapa
+Rapa
FSC.H
B.
MED21-FRB
+iMED21-FLAG
-Rapa
-β-Estradiol
+Rapa,
+β-Estradiol
iMED21-FLAG
iΔ3MED21-FLAG
iΔ5MED21-FLAG
FSC.H
C.
MED21
MED21-FRB
Δ3-MED21-FRB
Δ5-MED21-FRB
SDO
+Rapa
Count Distribution (Density)
Fluorescence (a.u.)
D.
MED21-FRB +
iMED21-FLAG
iΔ3-MED21-FLAG
iΔ5-MED21-FLAG
SDO
+Rapa
+β-estra
Fluorescence (a.u.)
E.
+Aux
ScMED21
ScMED21 FRB
AtN5 ScMED21 FRB
ARC (TPLN188)
Venus Fluorescence (a.u. x1000)
Time (min)
F.
+Aux
Growth (Cells x1000)
Time (min)

1177

1178 **Supplemental Figure 4. Inducible MED21 rescues rapamycin induced yeast growth**
1179 **defects. A.** Depletion of nuclear ScMed21 by Rapamycin increased cell size even in short time-
1180 courses, consistent with its essential role in many core pathways. Scatterplots of side scatter
1181 area by forward scatter height (SSC.A x FSC.H) indicate large scale increases in cell size in
1182 populations of yeast with (blue) or without (red) Rapamycin treatment. **B.** Inducible Med21
1183 (iMed21) wild type and variants cell size were examined before (red) and after (blue) treatment
1184 with Rapamycin and b-estradiol to simultaneously deplete the wild-type Med21-FRB fusion, and
1185 induce the transcription of the Med21 variant. Scatterplots of side scatter area by forward
1186 scatter height (SSC.A x FSC.H) demonstrate a less disrupted cell size compared to Anchor
1187 Away strains in (**A**). **C-D.** Histograms of Venus fluorescence in inducible Med21 (iMed21)
1188 strains demonstrate that populations were evenly distributed around a single mean, suggesting
1189 we were observing the immediate effects of the Med21 deletions. The histograms were built
1190 using ggplots Density function to create a visualization of count distribution. These samples
1191 were tested at 300 minutes (as in Figure 4D), and plotted to visualize cells at the equivalent
1192 stage of growth, Med21 depletion, and induction. **C.** Effect of anchor away of Med21-FRB
1193 variants alone and **D.** Depletion of ScMed21-FRB after induction (b-estradiol added 4 hours
1194 before Rapamycin treatment) of iMed21. **E**. Conversion of the first five amino acids of ScMed21
1195 to the corresponding sequence from AtMED21 results in an identical repression profile. Time
1196 course flow cytometry of SLARC strains following auxin addition. For all cytometry experiments,
1197 the indicated TPL construct is fused to IAA14, because this IAA performs better in haploid yeast
1198 strains that IAA3. Every point represents the average fluorescence of 5-10,000 individually
1199 measured yeast cells (a.u. - arbitrary units). Auxin (IAA-10μM) was added at the indicated time
1200 (gray bar, + Aux). Two independent experiments are shown for each construct. **F.** Cell growth of
1201 the strains in (**E**) indicate the swap of the N-terminal region had no effect on yeast growth or
1202 viability. Data presented is events per microliter over the time-course of the cytometry
1203 experiments. **C.** Protein expression analysis by western blotting of strains used in A & B. In this
1204 ARC, TPLN188-IAA3 is N-terminally fused to 2xHA. Total protein loading levels were tested by
1205 blotting against the housekeeping gene PGK1 (bottom panel).
1206
1207

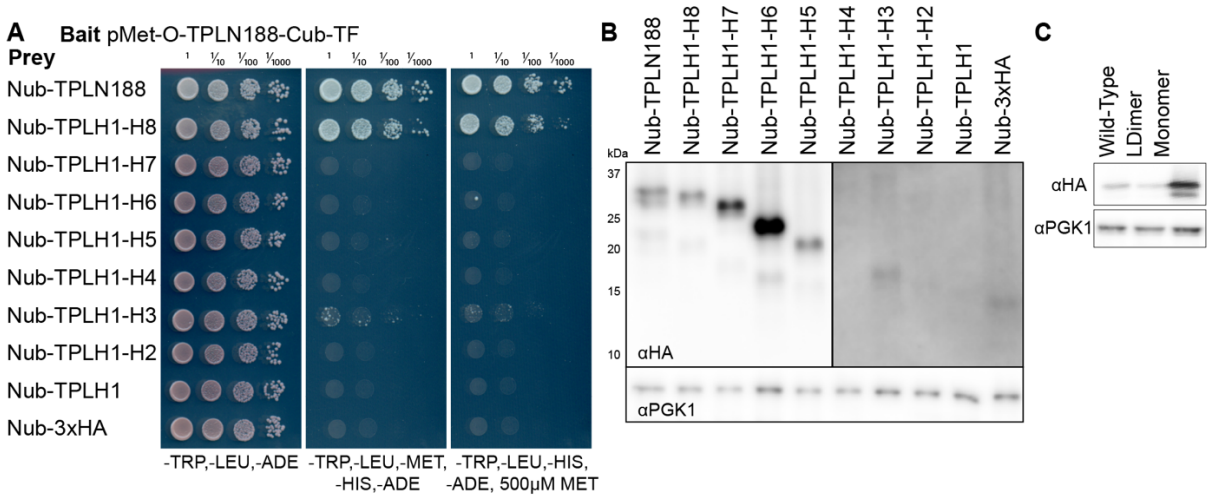


**Supplemental Figure 5. TPL multimerization requires Helix 8. A.** Cytoplasmic split ubiquitin interaction (cytoSUS) assay on serial deletions of TPL. Interaction of bait and prey proteins reconstitute split ubiquitin, release a synthetic transcription factor that allows growth on media lacking Histidine and Adenine. The expression level of the bait protein can be repressed through increased Methionine in the media. **B**. Protein levels of Nub-TPL fusions were tested by PAGE and western blotting for the c-terminal 3xHA epitope tag included in all constructs. Deletions longer than H1-4 are detectable at higher levels (left panel), whereas shorter isoforms required longer exposure times to detect (right panel). Total protein loading levels were tested by the housekeeping gene PGK1 (bottom panel). **C.** Protein expression analysis by western blotting of tetramerization mutants expressed in yeast for cytoSUS interaction assay in Figure 5I. Prey constructs are C-terminally fused to 2xHA. Total protein loading levels were tested by blotting against the housekeeping gene PGK1 (bottom panel).

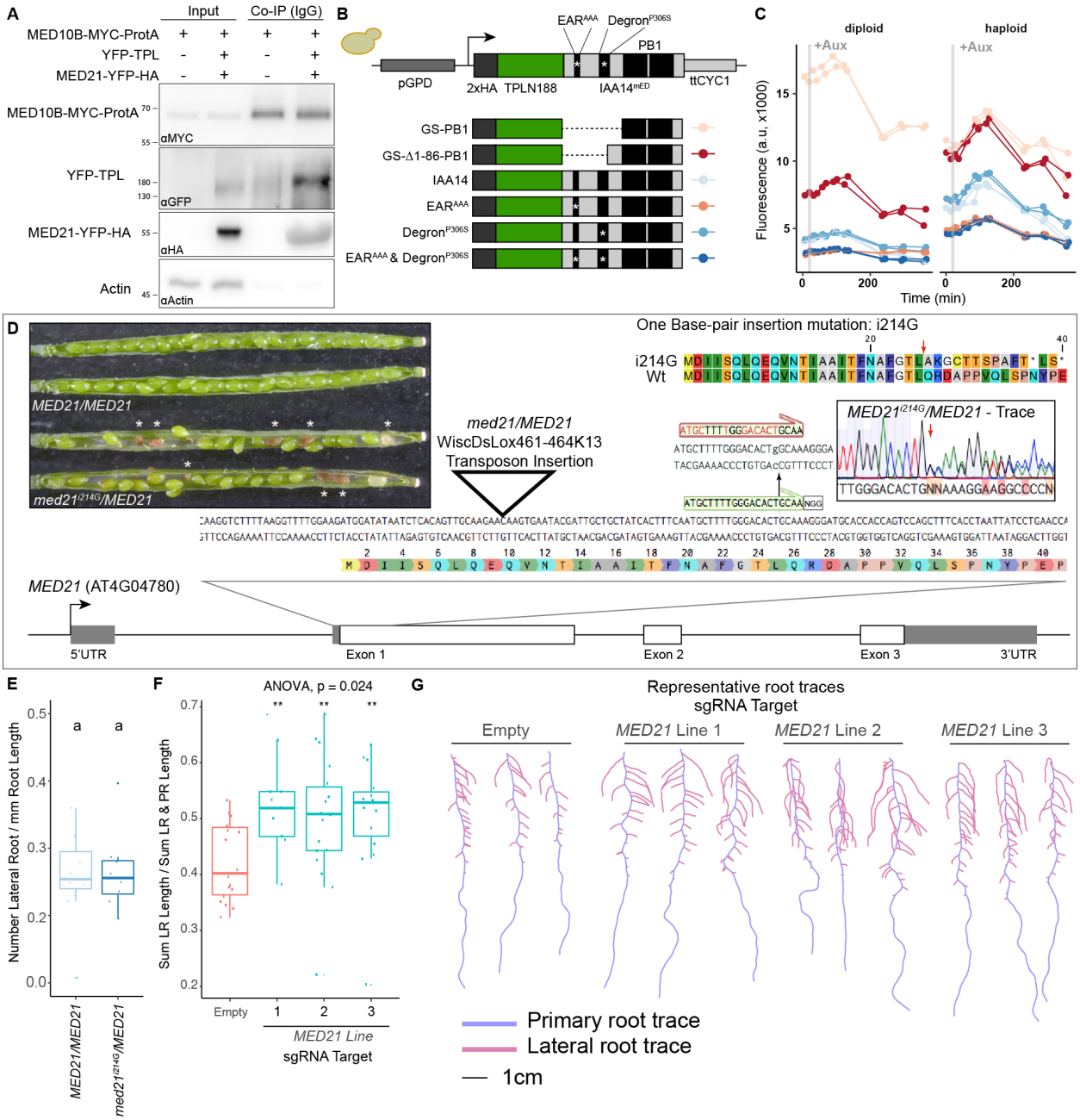


**Supplemental Figure 6. The TPL-MED21 interaction is required for repression in plants.** **A.** MED21 and TPL Co-Immunoprecipitated with AtMED10B from tobacco extracts. Each construct was expressed under the viral 35S promoter, and tissues were harvested after 2 days of injection. MED10B was purified by incubation with IgG sepharose beads (see methods), and the presence of interacting proteins was determined by western blotting. Actin was used as a control to determine the efficacy of washing. **B-C.** Engineering and prototyping a variant of TPLN-IAA14$^{mED}$ which carries mutations in the EAR domain (EAR$^{AAA}$) and in the degron (P306S) in yeast. **B.** Cartoon schematic of the mutations tested during prototyping of the

1232 TPLN188-IAA14mED construct. In each case the identical glycine-serine linker (GS) was used
1233 as the flexible linker between the 2xHA-TPLN188 protein and the portion of IAA14 retained in
1234 the construct. **C.** Time course flow cytometry of TPLN-IAA14$^{mED}$ strains following auxin addition.
1235 Strains containing the TPLN-IAA14$^{mED}$ was tested in both haploid and diploid strains and
1236 demonstrated similar repression profiles. Every point represents the average fluorescence of 5-
1237 10,000 individually measured yeast cells (a.u. - arbitrary units). Auxin (IAA-10μM) was added at
1238 the indicated time (gray bar, + Aux). Two independent experiments are shown for each
1239 construct. **D.** Identification and characterization of a novel CAS9-based insertional mutation in
1240 *MED21*. The *MED21* genomic locus (AT4G04780) is shown as a cartoon, with a zoom in on the
1241 beginning of the coding sequence highlighted with the amino acid sequence. The location of the
1242 *med21/MED21* mutant (WiscDsLox461-464K13, see triangle), and the sgRNA we employed
1243 (see green annotation and NGG PAM site) highlighted. The insertion of a G at nucleotide
1244 position +214 after the transcriptional start site abrogates the sgRNA site (red annotation above
1245 with i214G). A representative sequencing trace demonstrates the position where the
1246 heterozygote carries i215G, and the predicted effect to the coding sequence is shown at the top
1247 right – a red arrow indicates the first codon affected by the i214G mutation. The Inset pictures at
1248 the top left demonstrate the embryo lethality phenotype in *med21*$^{i214G}$*/MED21* heterozygote
1249 siliques. White asterisks indicate the embryos that have begun to degenerate. These aborted
1250 seeds are visibly brown indicating that fertilization took place allowing the seed coat to form
1251 before development failed. **E.** *med21*/*MED21* heterozygotes are haplo-sufficient for lateral root
1252 development. Lateral root density (number of lateral roots / primary root length) was calculated
1253 at 10 days post germination. Lower case letters indicate significant difference (ANOVA and
1254 Tukey HSD multiple comparison test; $p<0.001$). **F.** Ratio of lateral root lengths to total root
1255 lengths (lateral root lengths + primary root length) in dCAS9 repressor lines targeting *MED21*
1256 calculated at 10 days post germination. Statistical tests (ANOVA and Wilcox test) are reported
1257 above the graph. **G.** Representative root traces of dCAS9 repressor lines targeting *MED21*
1258 calculated at 10 days post germination.
1259